NAVAL POSTGRADUATE SCHOOL

MONTEREY, CALIFORNIA

THESIS

SUBTIDAL VARIABILITY IN THE NORTHERN SOUTH CHINA SEA DURING SPRING 2001

by

Megan D. Weller

June 2005

Thesis Advisor:	Steven R. Ramp
Second Reader:	Leslie K. Rosenfeld

THIS PAGE INTENTIONALLY LEFT BLANK

REPORT DOCUMENTATION PAGE	Form Approved OMB No. 0704-0188

1. AGENCY USE ONLY *(Leave blank)*	2. REPORT DATE	3. REPORT TYPE AND DATES COVERED
	June 2005	Master's Thesis

4. TITLE AND SUBTITLE: Subtidal Variability in the Northern South China Sea During Spring 2001	5. FUNDING NUMBERS
6. AUTHOR(S) Megan D. Weller	
7. PERFORMING ORGANIZATION NAME(S) AND ADDRESS(ES) Naval Postgraduate School Monterey, CA 93943-5000	8. PERFORMING ORGANIZATION REPORT NUMBER
9. SPONSORING /MONITORING AGENCY NAME(S) AND ADDRESS(ES) N/A	10. SPONSORING/MONITORING AGENCY REPORT NUMBER

11. SUPPLEMENTARY NOTES The views expressed in this thesis are those of the author and do not reflect the official policy or position of the Department of Defense or the U.S. Government.

12a. DISTRIBUTION / AVAILABILITY STATEMENT	12b. DISTRIBUTION CODE
Approved for public release; distribution is unlimited	

13. ABSTRACT (maximum 200 words)

The Asian Seas International Acoustics Experiment (ASIAEX) conducted in April and May of 2001 helped researchers take a major step in understanding the circulation of the northern South China Sea. This region crosses one of the primary sea lanes of communication between Chinese submarine bases and the Pacific theater, therefore making it an extremely valuable source of knowledge for the United States Navy. This thesis provides a qualitative and quantitative analysis of the mesoscale variability in the South China Sea during spring 2001 using observational data from the ASIAEX experiment.

An array of moorings (S1-S8) equipped with ADCPs, pressure gauges, temperature and salinity sensors, and current meters, was placed between the southern tip of Taiwan and Dongsha Island (Pratis Reef). Data results show that significant mesoscale features existed in the South China Sea. Mean currents over the continental shelf were found to be primarily wind driven while flows over the continental slope were forced by the mesoscale features. The South China Sea Warm Current was observed twice over the slope during ASIAEX. A cyclonic meander of the northern gyre propagated onshore and southwest near S7. Tropical Cyclone Cimaron set up a pressure driven flow towards the southwest along the continental shelf, suggesting that a storm this size can influence the circulation in the entire South China Sea.

Model results from the Northern South China Sea Nowcast/Forecast System were compared to the observational data. The model gave a good description of the big picture in the South China Sea but was unable to resolve the smaller-scale events. The model was too constrained by topography and had a distinct offset of the alongshore component most likely imposed on by open boundary forcing.

14. SUBJECT TERMS South China Sea, Asian Seas International Acoustics Experiment (ASIAEX), Subtidal variability	15. NUMBER OF PAGES 83
	16. PRICE CODE

17. SECURITY CLASSIFICATION OF REPORT	18. SECURITY CLASSIFICATION OF THIS PAGE	19. SECURITY CLASSIFICATION OF ABSTRACT	20. LIMITATION OF ABSTRACT
Unclassified	Unclassified	Unclassified	UL

NSN 7540-01-280-5500 Standard Form 298 (Rev. 2-89)
Prescribed by ANSI Std. 239-18

THIS PAGE INTENTIONALLY LEFT BLANK

Approved for public release; distribution is unlimited

SUBTIDAL VARIABILITY IN THE NORTHERN SOUTH CHINA SEA DURING SPRING 2001

Megan D Weller
Ensign, United States Navy
B.S., United States Naval Academy, 2004

Submitted in partial fulfillment of the
requirements for the degree of

MASTER OF SCIENCE IN APPLIED SCIENCE
(PHYSICAL OCEANOGRAPHY)

from the

NAVAL POSTGRADUATE SCHOOL
June 2005

Author: Megan D. Weller

Approved by: Steven R.Ramp
Thesis Advisor

Leslie K. Rosenfeld
Second Reader

Mary L. Batteen
Chairman
Department of Oceanography

Donald P. Brutzman
Chair
Undersea Warfare Academic Committee

THIS PAGE INTENTIONALLY LEFT BLANK

ABSTRACT

The Asian Seas International Acoustics Experiment (ASIAEX) conducted in April and May of 2001 helped researchers take a major step in understanding the circulation of the northern South China Sea. This region crosses one of the primary sea lanes of communication between Chinese submarine bases and the Pacific theater, therefore making it an extremely valuable source of knowledge for the United States Navy. This thesis provides a qualitative and quantitative analysis of the mesoscale variability in the South China Sea during spring 2001 using observational data from the ASIAEX experiment.

An array of moorings (S1-S8) equipped with ADCPs, pressure gauges, temperature and salinity sensors, and current meters, was placed between the southern tip of Taiwan and Dongsha Island (Pratis Reef). Data results show that significant mesoscale features existed in the South China Sea. Mean currents over the continental shelf were found to be primarily wind driven while flows over the continental slope were forced by the mesoscale features. The South China Sea Warm Current was observed twice over the slope during ASIAEX. A cyclonic meander of the northern gyre propagated onshore and southwest near S7. Tropical Cyclone Cimaron set up a pressure driven flow towards the southwest along the continental shelf, suggesting that a storm this size can influence the circulation in the entire South China Sea.

Model results from the Northern South China Sea Nowcast/Forecast System were compared to the observational

data. The model gave a good description of the big picture in the South China Sea but was unable to resolve the smaller-scale events. The model was too constrained by topography and had a distinct offset of the alongshore component most likely imposed on by open boundary forcing.

TABLE OF CONTENTS

THIS PAGE INTENTIONALLY LEFT BLANK

LIST OF FIGURES

THIS PAGE INTENTIONALLY LEFT BLANK

LIST OF TABLES

THIS PAGE INTENTIONALLY LEFT BLANK

ACKNOWLEDGMENTS

I would like to thank my thesis advisor, Dr. Steven R. Ramp for helping me through every step of the thesis process. I would also like to thank Fred Bahr for being so helpful and understanding when it came to using Matlab. I could not have done this thesis without their support.

THIS PAGE INTENTIONALLY LEFT BLANK

I. INTRODUCTION

A. BACKGROUND

In the spring of 2001, The Asian Seas International Acoustics Experiment (ASIAEX) maintained an array of moorings located between the southern tip of Taiwan and Dongsha (Pratis) Island. The moorings were positioned along the continental shelf break in an area enclosed by 21 to 22.5°N, 117 to 119°E (Ramp et al., 2004). Seven moorings (S2-S8) were located in this region, positioned in an across shelf line spanning from 80 m to 350 m depth (Figure 1).

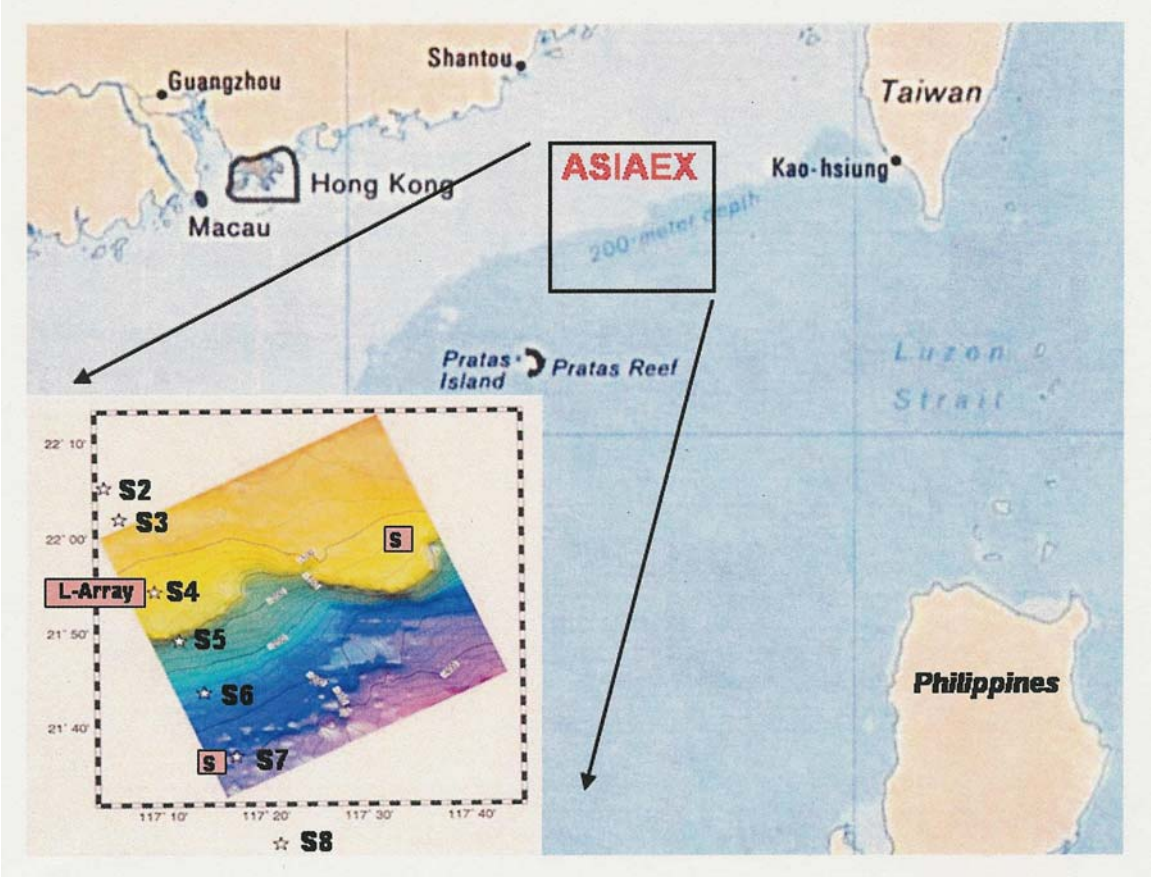

Figure 1. Locator map showing the positions of the ASIAEX moorings. The current meter moorings are indicated by stars labeled S2-S8. (From: Ramp et. al., 2004)

The ADCP at mooring S8 failed and therefore will not be included in this paper. Data from the moorings were collected during April and May 2001 and consisted of water property measurements including temperature, salinity, and velocity. Measurements were collected using temperature, temperature/conductivity, current meter, and ADCP instruments suspended in the water column at each mooring (Figure 2). More information regarding the details of individual moorings can be found in Ramp et al.(2004).

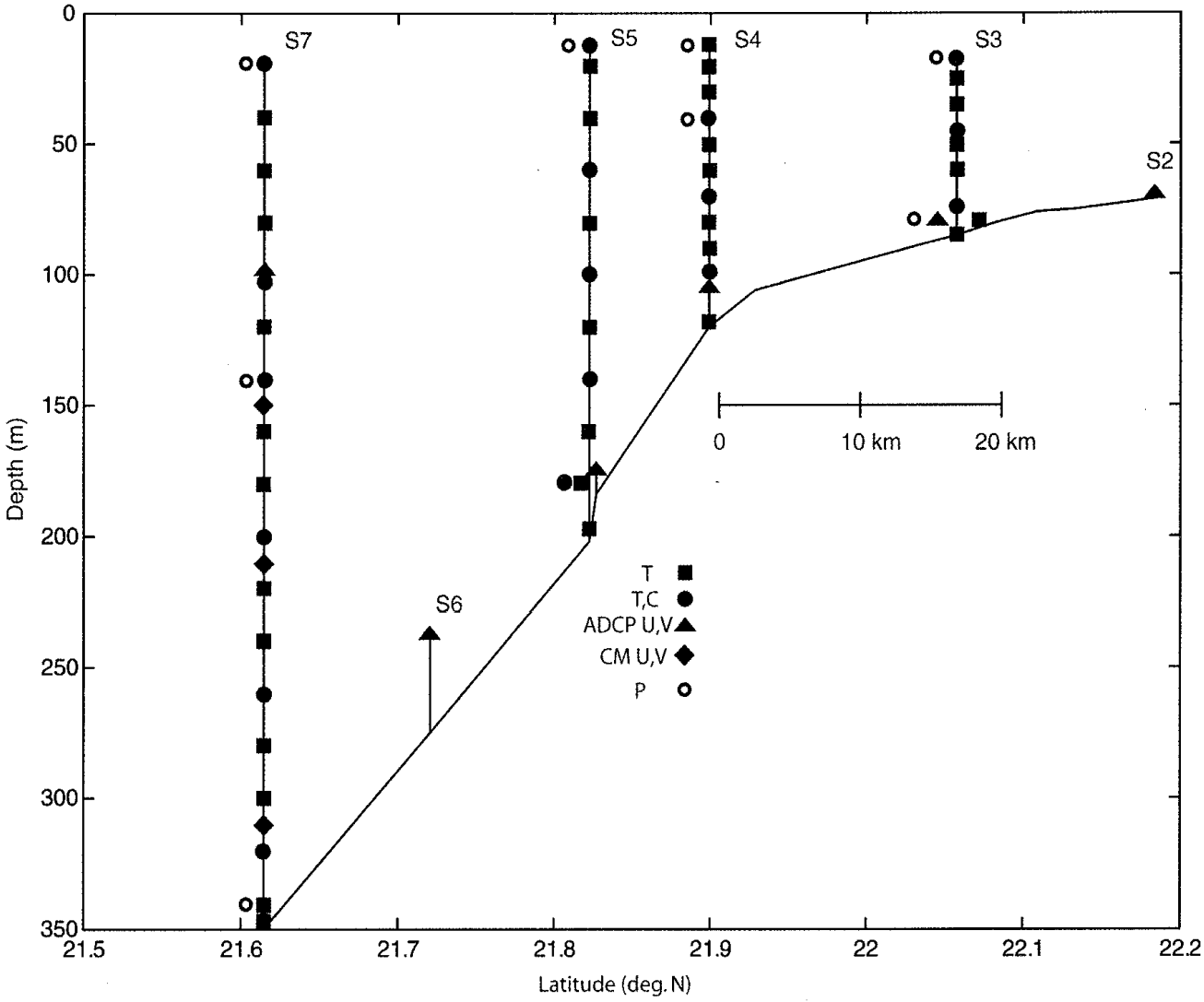

Figure 2. A cross-section of the oceanographic moorings showing the placement of the temperature, temperature/conductivity, current meter, and ADCP instruments in the water column. (From: Ramp et. al., 2004)

The South China Sea is part of a group of marginal seas located in the western Pacific Ocean which are connected through small passages such as the Taiwan and Tsushima Straits (Figure 3). It is 2,775 km long, 890 km wide and encompasses a surface area of 3×10^6 km^2. A wide

continental shelf that spans 220 km and has a depth of less than 100 m can be found off the southeast coast of China from Vietnam to Taiwan. A maximum depth of 4500 m is located in the center of the basin. The Indonesian Sea lies to the south, the East China Sea to the north, and the Philippine Sea lies to the west. The Luzon Strait connects to the Philippine Sea between the islands of Taiwan and Luzon. At the entrance, the Luzon Strait is 250 km wide and has a sill depth of 1900 m, but there are many shallower passages around the Batan Islands group. The vast width and depth of the Luzon Strait makes it the leading strait for mass transport. The Luzon Strait is also a major source of ventilation for the South China Sea. The Taiwan Strait is located between mainland China and Taiwan. This shallow (< 100 m) strait does not have nearly the same influence as the Luzon Strait but is important in terms of its fresh water input as well as its influence on the semidiurnal tides (Beardsley et al. 2004; Ramp et al., 2004). Other straits also connect the South China Sea to surrounding bodies of water but do not influence the ASIAEX area and are therefore not emphasized in this paper.

Figure 3. Locator map of the Northwest Pacific region including marginal seas and straits that influence the South China Sea. (AFTER: base map http://www.eia.doe.gov/emeu/cabs/schina.html), last accessed June 2005).

B. CIRCULATION IN THE SOUTH CHINA SEA

The low frequency circulation in the South China Sea is driven mainly by seasonally varying wind patterns. Most influential are the reversing monsoonal winds between

summer and winter, and the formation of monsoon depressions. The summer monsoon lasts from June to September producing winds that blow from the southwest resulting from an intense low pressure system over Asia. The SW monsoon reaches its maximum wind strength in August (Shaw and Chao, 1994; Ramp et al., 2004). The months of October and November show a transition period for the direction of the winds. December brings the winter monsoon which lasts until March and produces winds blowing from the northeast stemming from a high pressure system over Asia. The winter monsoon is the stronger of the two and develops in the northern part of the basin and then spreads southward. In April and May the winds die down and another transition period between the two monsoons can be seen (Shaw and Chao, 1994; Ramp et al., 2004). The sea state is at its calmest during the transition period, and the ASIAEX program used this time frame to conduct the experiment.

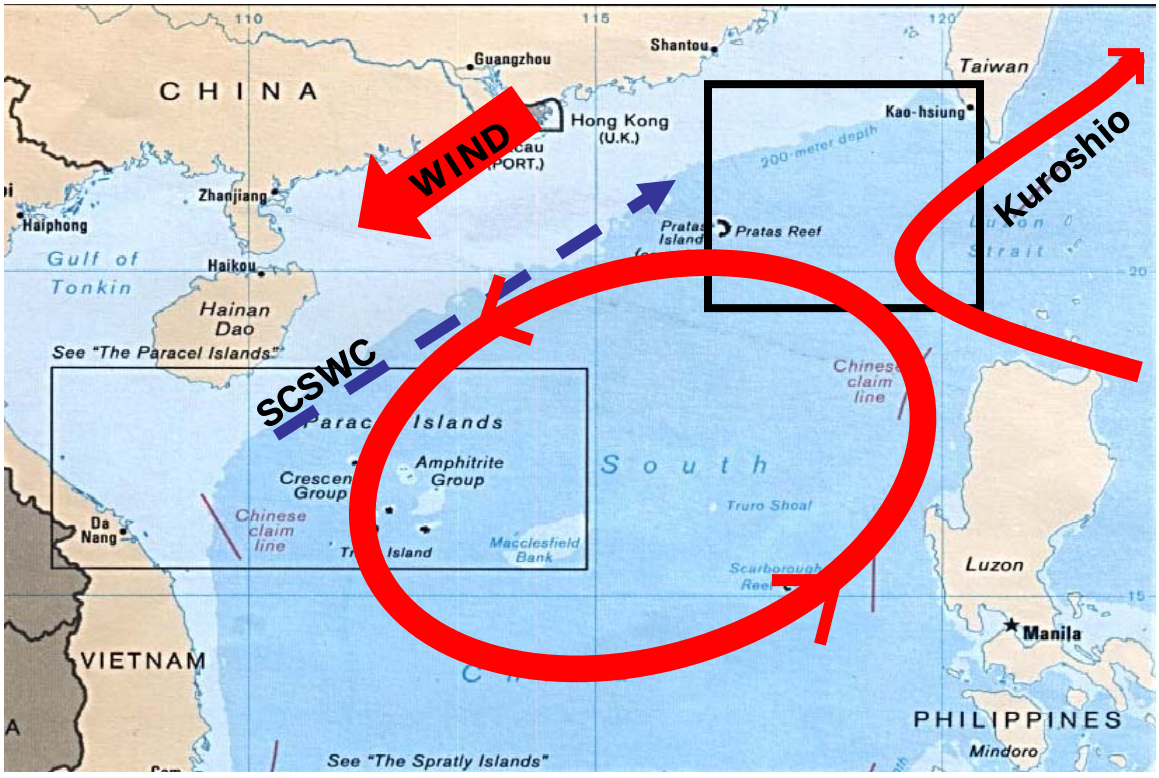

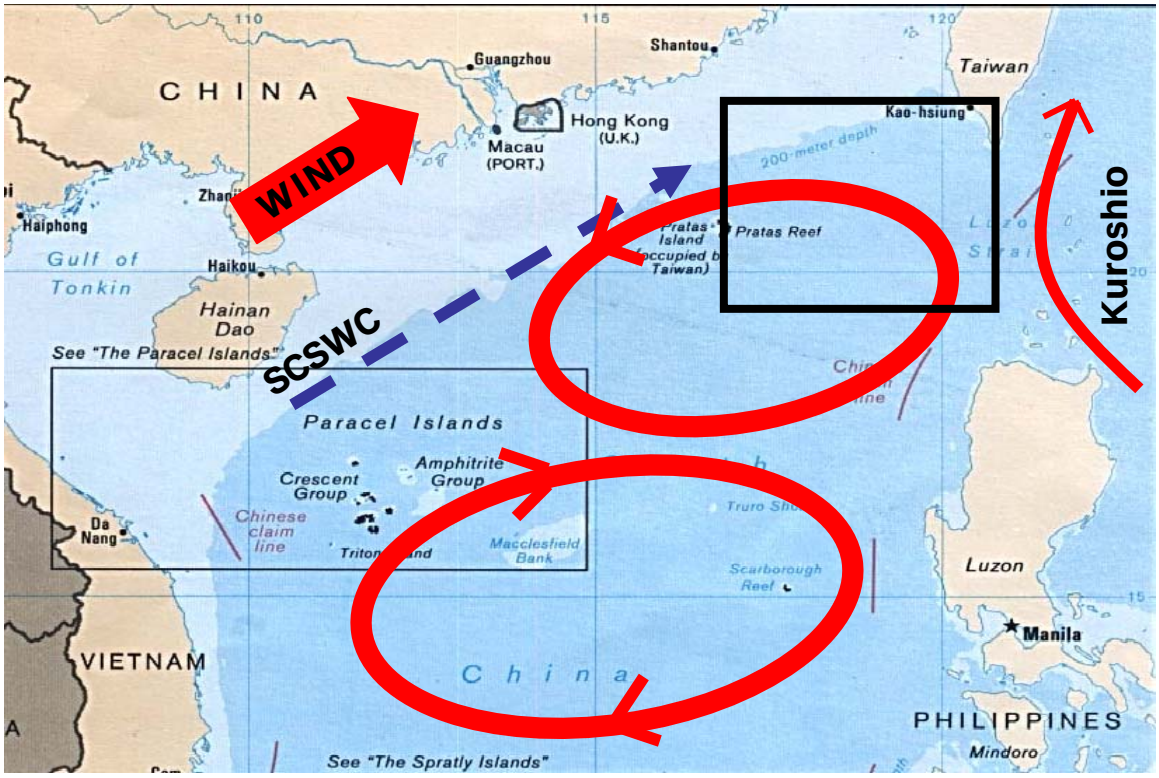

Figure 4. General flow maps showing common circulation patterns during the (a) winter months and (b) summer months in the South China Sea. The black box indicates the NSCSNFS model domain. (After: base map, http://www.lib.utexas.edu/maps/middle_east_and_asia/schina_sea_88.jpg, last accessed May 2005).

The monsoon winds produce seasonal circulation patterns in the South China Sea. During the winter months in the South China Sea winds drive the basin in a cyclonic gyre that covers the entire sea. During the summer months two gyres co-habit the South China Sea, a cyclonic gyre to the north and an anti-cyclonic one to the south (Figure 4). ASIAEX occurred during the transition period between these two seasonal flows, 21 April through 17 May. As the transition between winter and summer develops, the cyclonic gyre is pushed northward and the anti-cyclonic gyre begins to develop in the southern part of the South China Sea

[Chapman et. al., 2004]. The cyclonic gyre being pushed north manifests itself as a steady southwestward flow developing over the slope during the length of the experiment. A model representation of the transition between the two gyres is shown in Figures 5 and 6 [Chapman et. al., 2004]. The model used by Chapman et. al., 2004 was the Northern South China Sea Nowcast/Forecast System (NSCSNFS). This model will be discussed subsequently in the model/data comparisons section. The first figure shows model results from February through May. As can be seen by the surface velocity vectors and salinity change, the cyclonic gyre discussed above is definitely spreading northward in the model. In February and May the northern edge of the cyclonic gyre extends just past 20°N while during the months of April and May it extends all the way to 21.5°N. The second figure shows model results from the February and May, or winter period and transition period of the seasonal flow. Results for the surface and 100 m depth are shown on each date. Knowing the wind stress at Dongsha Island (Figure 11), it can be inferred from the figure that wind driven flows were produced near the surface while the mesoscale dominated at 100 m depth. Chapman’s figures suggest the general subsurface flow should be alongshore to the southwest. The surface flow is wind driven and therefore does not follow this pattern.

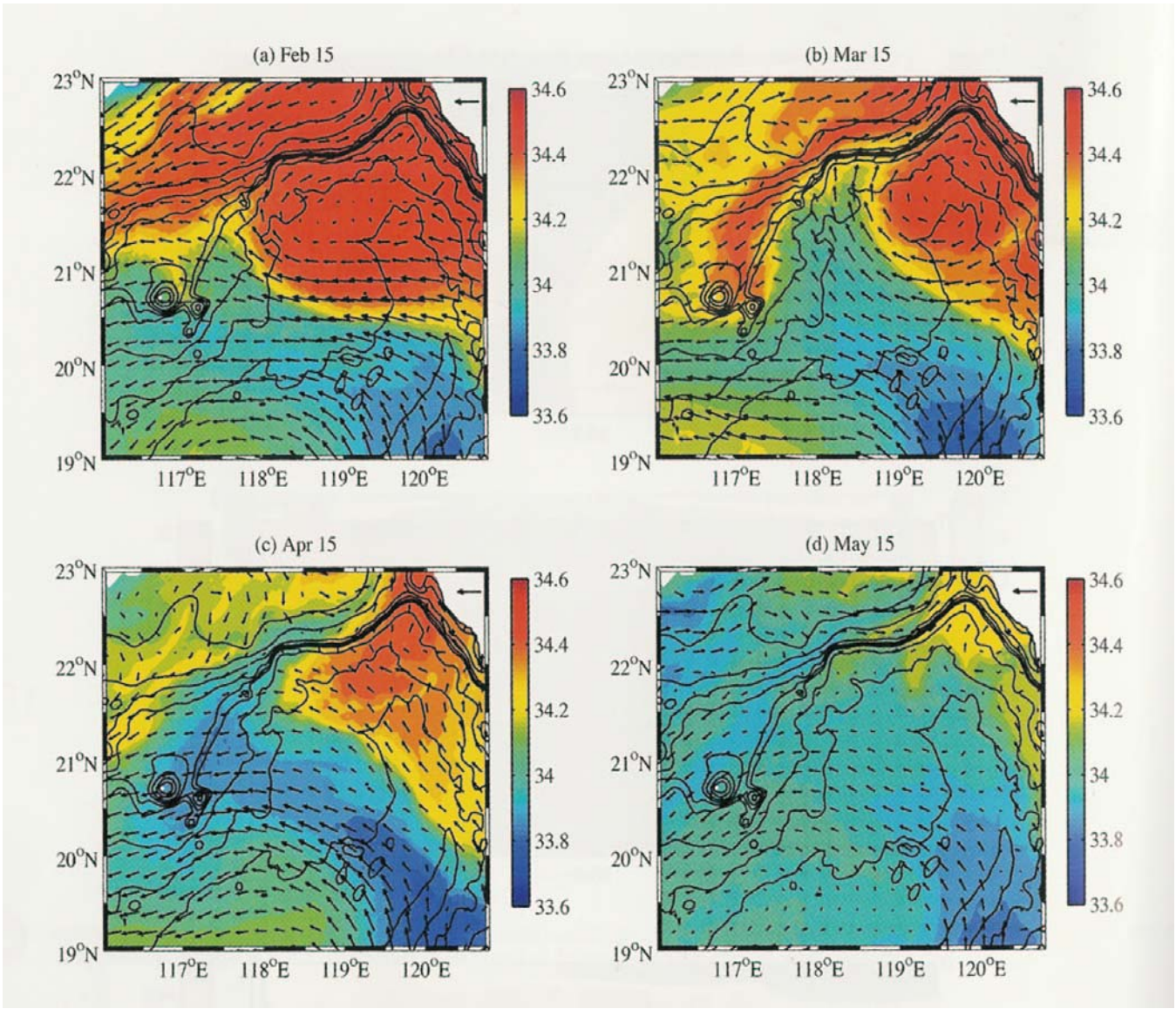

Figure 5. Surface velocity vectors and salinity at four times during the 2001 full-model calculation. The vector scale plotted on Taiwan is 0.5 m/s. Salinity scale is shown at the right in psu. Black contours show the 50, 100, 200, 300, 400, 500, 1000, 2000, 3000, and 4000 m isobaths. (a) 15 February; (b) 15 March; (c) 15 April; (d) 15 May (From: Chapman et. al, 2004)

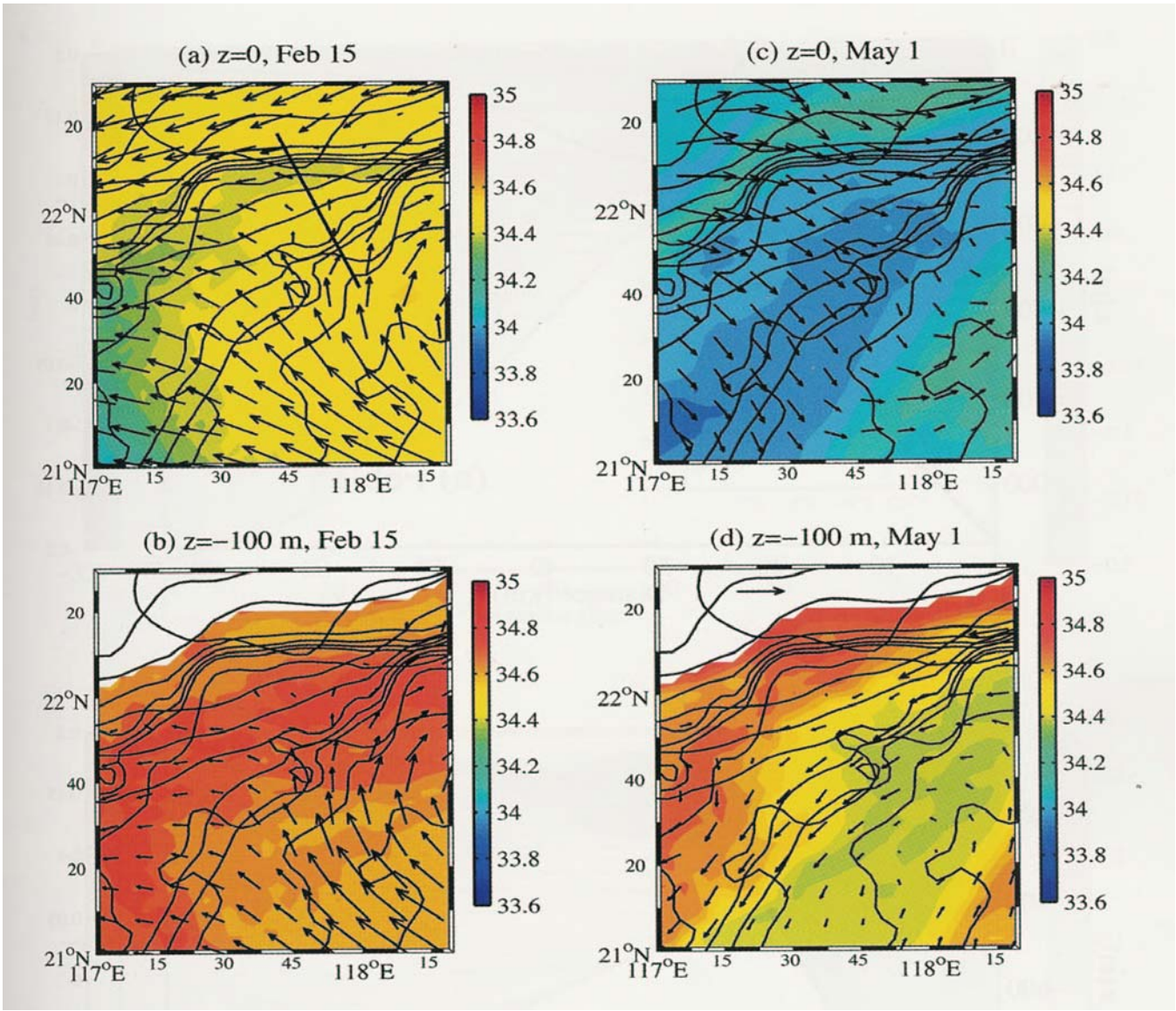

Figure 6. Velocity vectors and salinity within the ASIAEX area, at the surface and at 100 m depth on both February 15 and May 1 of the 2001 full-model calculation. The vector scale plotted in the white regions of (d) is 0.3 m/s. Salinity scale is shown at the right in psu. Black contours show the 50, 100, 200, 300, 400, 500, 1000, 2000, 3000, and 4000 m isobaths. (a) z = 0 m, 15 February; (b) z = -100 m, 15 February; (c) z = 0 m, 1 May; (d) z = -100 m, 1 May. (From: Chapman et. al, 2004)

Monsoon depressions intermittently dominate the wind patterns of the South China Sea. They usually occur in the

summer months between May and September and have averaged approximately 4 monsoonal depressions per year (Ramp et. al, 2004). They are most frequently observed in August and September, however the summer of 2001 proved anomalous and a monsoonal depression formed during the ASIAEX experiment in April. The monsoonal depression eventually formed into tropical storm Cimaron (Figure 7). The cyclone’s path came through the Philippine Islands and up the western boundary of the island of Luzon, eventually heading back out to the Philippine Sea by way of the Luzon Strait. Despite just grazing the mooring line, this storm had a major impact on the ASIAEX currents and will be described further in the discussion section.

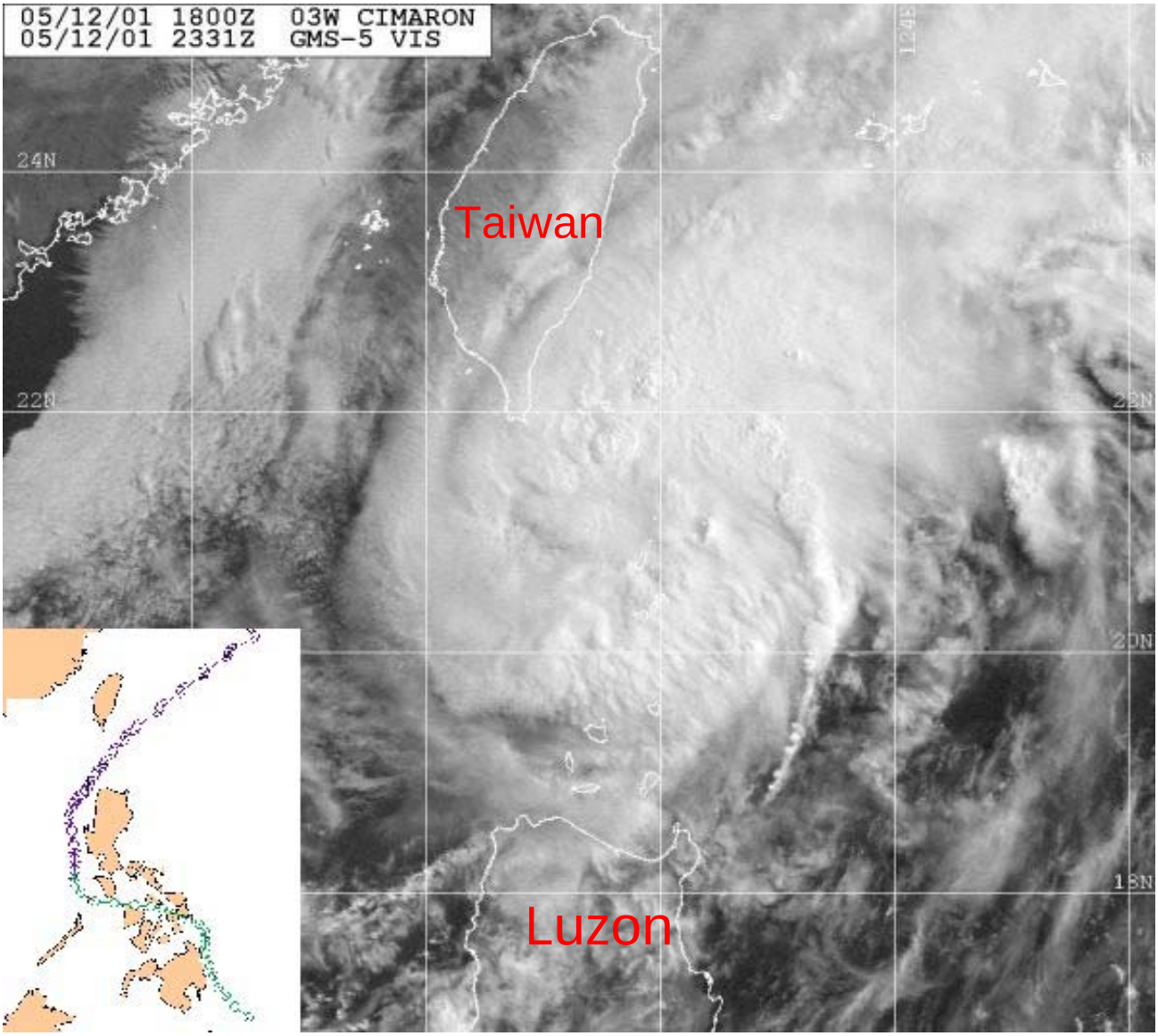

Figure 7. Visual image of tropical cyclone Cimaron as it is exiting the South China Sea through the Luzon Strait on its way into the Philippine Sea. The insert shows the path Cimaron took as it traveled through the South China Sea(After: base map from http://www.npmoc.navy.mil/jtwc/atcr/2001atcr/ch1/chap1_page10.html, last accessed June 2005).

The majority of water exchange between the South China Sea and its surrounding bodies of water takes place through the Luzon Strait (Figure 3). The sill depth of 1900 m blocks the abyssal waters of the Philippine Sea from

flowing into the South China Sea but the remaining water masses show an exchange between the two seas. Potential temperature-salinity analysis shows that Deep Water of the West Philippine Sea eventually forms the bottom water of the South China Sea (Su, 1998). This is what one would expect to find considering the small amount of water exchange between the South China Sea and its surrounding bodies of water, mainly due to shallow sill depths and narrow passages. Analysis from Su (1998) also supports the belief that tropical and Intermediate water above 600 m depth intrude into the South China Sea as far in as the continental slope. Residence time for this bottom water averages from 40-115 years. Short residence times result from rapid flushing and rarely exceed 100 years (Broecker et al., 1986). Transport through the Luzon Strait is governed by the seasonal variability in the monsoon winds. A pressure gradient develops in response to the winds, producing a pressure head at the Luzon Strait during the Southwest monsoon and a deficit during the northwest monsoon, affecting the amounts of water exchanged (Centurioni et al., 2004; Metzger and Hurlbert, 1996).

Surface currents in the South China Sea were first observed by Wyrtki (1961). A southward western boundary current occurs off Vietnam in the summer while a northward western boundary current occurs in the winter. The development and intensity of these surface currents can be explained by the monsoonal winds affecting the area. The most influential surface current is the Kuroshio Current whose extent of intrusion in the South China Sea has caused much debate. As the North Equatorial Current flows northwest along the Philippines, it develops into the

Kuroshio Current. This current continues across the Luzon Strait and up the eastern side of Taiwan. Sometimes the current extends into the South China Sea basin as it enters just north of Luzon and exits just south of Taiwan. The extent to which the waters of the Kuroshio Current enter the South China Sea varies seasonally and inter-annually. When Kuroshio water does enter the South China Sea it becomes known as the Kuroshio Intrusion (Metzger and Hurlburt, 1996). Theoretically the Kuroshio Intrusion is most dominant during the fall and winter months but has also been seen during the summer (Shaw and Chao, 1994). The most recent results suggest intrusions occur in fall only (Centurioni et al, 2004). The less likelihood of the Kuroshio Intrusion occurring during the summertime could be due to the build up of water at the Luzon Strait created during the south-west monsoon. When the Kuroshio does intrude into the South China Sea, it creates a branch of water that initially flows toward the northwest but then turns southwest along the topography. As the monsoonal winds transition into the SW monsoon the Kuroshio Branch, now a water mass, is pushed northward toward the Taiwan Strait. The Kuroshio Branch does not act the same way every time. When the Kuroshio Intrusion hits the continental shelf, part of the intrusion might break off and flow southwest along the shelf break. Rarely, the Kuroshio Intrusion may pinch off and form large warm core rings (Ramp et al., 2004). The salinity of the Kuroshio Intrusion is a consistent maximum of 34.5 – 34.8 psu at 150 m water depth and therefore can be traced in the South China Sea (Ramp et al., 2004).

The South China Sea Warm Current (SCSWC) also varies seasonally and is a current that could potentially affect the ASIAEX region. Occurring during the relaxation of the NE Monsoon, the SCSWC originates off the coast of Vietnam and reaches as far north as the southern Taiwan Strait (Chao et al., 1994). The current spans alongshore a distance of 600-700 km and is 160-300 km wide extending down to 300 m depth. The relaxation of the SW monsoon would seem to enhance the currents existence (Chao et al., 1994). The wind relaxation sets up a pressure gradient along the northwestern boundary of the South China Sea, with sea level higher in the southwest than in the northeast. In other words, winds of the monsoon push water to the southwest. When the wind relaxes a return current is triggered as the sea level drops back to its original state (Chao et al., 1994). This mechanism suggests a current which may often be subsurface during times when the surface winds oppose it such a flow.

THIS PAGE INTENTIONALLY LEFT BLANK

II. DATA COLLECTION

A. CURRENT METER DATA

Current meter data was collected at six mooring stations (S2-S7) in the across shore direction extending over the continental shelf of the South China Sea. Moorings S3, S4, S5, and S7 were deployed by the Naval Postgraduate School, while moorings S2, and S6 were deployed by the National Taiwan University. Placements of temperature, temperature/conductivity, current meter, and Acoustic Doppler Current Profiler (ADCP) instruments were chosen (Figure 2 and Table 1) to resolve the vertical structure of internal waves (Ramp et al., 2004). Bottom depths ranged from 72 m at mooring S2 to 350 m at mooring S7. Mooring S3 contains data for half the time period due to fishing activity in the area which cut the mooring in half. The top half was visually sighted by the research vessel OCEAN RESEARCHER 1 (OR1) and the bottom half was recovered by dragging. Despite the moorings being deployed in an intense fishing area there was a high survival rate and therefore an almost complete data set was recovered for the across- shore line (Ramp et al., 2004). Mooring S5 was a narrowband 150 kHz ADCP with 8 m bins while S6 was a broadband 150 kHz ADCP with 10 m bins. ADCP’s at the remaining moorings (S2, S3, S4 and S7) were broadband units with bin lengths of 4 m at a frequency of 300 kHz. The data at these moorings were less contaminated by surface side-lobe reflection than the 150 kHz instruments.

Mooring	Latitude	Longitude	Bottom Depth (m)	Instr. Depth (m)	Start	Stop	Record Length (days)	sample Interval (min)
S8	*20 53.00*	*117 33.986*	*790*					
SeaCAT (TCP)				215	4/23/2001	5/21/2001	27.8	2
S7	*21 36.871*	*117 16.975*	*350*					
MicroCAT (TCP)				20	4/21/2001	5/18/2001	27.9	1
Starmon-mini				40	4/21/2001	5/18/2001	27.9	1
Starmon-mini				60	4/21/2001	5/18/2001	27.9	1
Starmon-mini				80	4/21/2001	5/18/2001	27.9	1
SeaCat				100	No Data			
ADCP BB 300 kHz/4 m				100	4/21/2001	5/19/2001	27.9	1
Starmon-mini				120	4/21/2001	5/18/2001	27.9	1
MicroCAT (TCP)				140	4/21/2001	5/18/2001	27.9	1
Aanderra RCM 8				150	4/21/2001	5/18/2001	27.9	2
Starmon-mini				160	4/21/2001	5/18/2001	27.9	1
Starmon-mini				180	4/21/2001	5/18/2001	27.9	1
MicroCAT (TC)				200	4/21/2001	5/18/2001	27.9	1
Aanderra RCM 8				210	4/21/2001	5/18/2001	27.9	2
Seamon-mini				220	4/22/2001	5/18/2001	26.5	2
Seamon-mini				240	No Data			
MicroCAT				260	4/21/2001	5/18/2001	27.9	1
Seamon-mini				280	4/22/2001	5/18/2001	26.5	2
Seamon-mini				300	4/22/2001	5/18/2001	26.5	2
Aanderra RCM 8				310	4/21/2001	5/18/2001	27.9	2
SeaCAT (TC)				320	4/21/2001	5/18/2001	27.9	1
Seaguage SBE26 (TP)				344	4/21/2001	5/18/2001	27.9	5
Seamon-mini				356	4/22/2001	5/18/2001	26.5	2
S6	*21 43.24*	*117 14.60*	*275*					
ADCP BB 150 kHz/10 m				240	4/21/2001	5/19/2001	28	2
SeaCAT (TCP)				245	4/21/2001	5/19/2001	28	2
S5	*21 49.346*	*117 12.328*	*202*					
MicroCAT (TCP)				12	4/21/2001	5/18/2001	27	1
Seamon-mini				20	Bad Data			
Seamon-mini				40	4/22/2001	5/18/2001	25.8	2
MicroCAT (TC)				60	4/21/2001	5/18/2001	27	1
Seamon-mini				80	4/22/2001	5/12/2001	20.29	2
MicroCAT (TC)				100	4/21/2001	5/18/2001	27	1
Seamon-mini				120	Bad Data			
MicroCAT (TC)				140	4/21/2001	5/18/2001	27	1
Seamon-mini				160	4/22/2001	5/18/2001	25.8	2
MicroCAT (TC)				180	4/21/2001	5/18/2001	27.02	1
Seamon-mini				197	No Data			
S5a	*21 49.616*	*117 12.240*	*184*					
ADCP NB 150 kHz/8 m				177	4/21/2001	5/18/2001	27.1	2
Seamon-mini				180	4/22/2001	5/18/2001	25.9	2
S4	*21 53.944*	*117 10.619*	*120*					

SBE 39 (TP)				11	4/21/2001	5/19/2001	27.8	0.5
Mini-Starmon				20	4/21/2001	5/19/2001	27.8	1
Mini-Starmon				30	Bad Data			
MicroCAT (TCP)				40	4/21/2001	5/19/2001	27.8	1
Seamon-mini				50	No data			
Seamon-mini				60	4/22/2001	5/19/2001	26.8	2
MicroCAT (TC)				70	4/21/2001	5/19/2001	27.8	1
Seamon-mini				80	4/22/2001	5/19/2001	26.8	2
Seamon-mini				90	4/22/2001	5/19/2001	26.8	2
MicroCAT (TC)				100	4/21/2001	5/19/2001	27.8	1
ADCB BB 300 kHz/4 m				104	4/21/2001	5/19/2001	27.8	1
Seamon-mini				118	Bad Data			
S3	*22 03.445*	*117 06.423*	*85*					
MicroCAT TCP				17	4/20/2001	5/5/2001	14.6	1
Seamon-mini				25	No Data			
Mini-Starmon				35	4/20/2001	5/5/2001	14.6	1
MicroCAT TC				45	4/20/2001	5/5/2001	14.6	1
Seamon-mini				50	Lost			
Seamon-mini				60	Lost			
MicroCAT TC				75	4/20/2001	5/5/2001	14.6	1
Seamon-mini				77	Lost			
ADCP BB 300/4 m				80	4/20/2001	5/5/2001	14.6	1
Seaguage SBE26 P				81	4/20/2001	5/21/2001	31	5
S2	*22 11.14*	*117 03.49*	*70*					
ADCP BB 300 kHz/4 m				72	4/20/2001	5/17/2001	26.5	2

Table 1. Mooring locations and instrument depths for all the environmental moorings deployed during ASIAEX. (From: Ramp et. al, 2004)

B. FILTERING

Sampling rates of the instruments were set as high as possible within limitations determined by power and internal memory. Supplementary external battery packs were installed to facilitate the high sampling rates of the instruments for one month. The ADCP sampled every second and averaged to 1 minute, while the T, TP, and TCP sensors sampled at one-minute intervals. The Aanderra current meters recorded vector averages at two minute intervals while the Seaguage SBE26 pressure sensor had a sampling

rate of five minutes (Ramp et al., 2004). Sampling started on 21 April 2001 and lasted until the instruments were recovered on 18 May 2001. Therefore, an average of 27 days worth of data were collected and recorded.

In order to analyze the data, the time series were digitally filtered into three bands. These bands consisted of the internal wave band, the tidal band, and the low-frequency (LF) or mesoscale band (Ramp et al., 2004). This paper will only look at the low-frequency mesoscale band. The data were filtered through a well-known low-pass filter with a half-power point at forty-six hours (Denbo et al., 1984) to separate the mesoscale variability from the tidal, inertial, and higher-frequency motions.

III. RESULTS

A. MEAN CURRENTS

Mean currents and principal axes for currents observed at 30 m, 50 m, 90 m and 150 m depth summarize the flow throughout the water column (Figures 8 and 9). The mean currents were onshore at S2 with flow steadily becoming more alongshore over the upper slope to S7. At moorings S2 and S3, the bottom depth only reached a maximum of 85 m, and the currents generally followed the winds. S4 was located on the upper slope and as a result was representative of the transition between shelf and slope water. The mean vector at S4 was onshore at 30 and 50 m depth, more alongshore near the bottom at 90 m depth. Mean flows at moorings S5, S6, and S7 were mostly alongshore with the exception of a mid-water cross-shore flow at S5. These moorings, S5 through S7, reached a maximum depth of 350 m over the continental slope; therefore the mean flow direction was influenced more by topography than by wind stress. The influence of topography can be seen in the figures as depth increases. At 30 m and 50 m depth across-shore flow was observed at S2, S3 and S4. At 90 m depth S4 became alongshore as it felt the effects of bottom topography, while S5 was still across-shore because 90 m was still mid-water column for this mooring. Finally at 150 m depth all moorings over the slope were influenced by topography and therefore had alongshore flow. Figures 8 and 9 give a good representation of how flow coming into the ASIAEX area followed the northern edge of the northern cyclonic gyre until it was influenced by topography at depth.

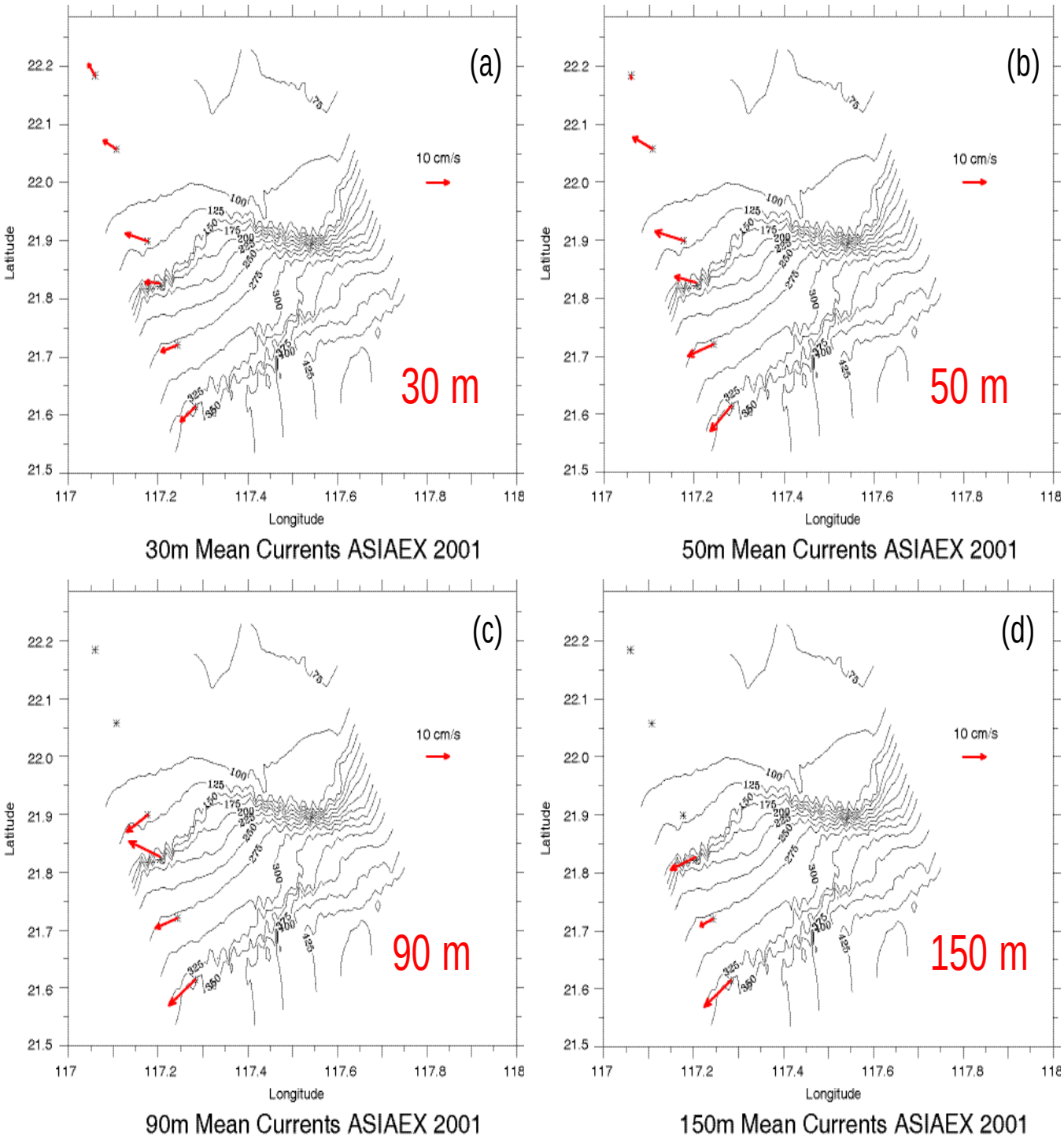

Figure 8. Map showing the mean currents at each mooring, S2-S7. Depths of 30 m (a), 50 m (b), 90 m (c), and 150 m (d) are shown. The black solid lines are contour lines mapping the sea floor in the ASIAEX region.

The principal axis figure shows the standard deviation ellipses about the mean. The major and minor axis of the ellipse show larger current fluctuations at the shelf moorings, S2-S4, than at the moorings over the slope. Also as depth increased from 30 m to 150 m, the standard deviation decreased at all moorings. Over the shelf, the standard deviation exceeds the mean, indicating the mean direction was not well resolved by these short records. Over the slope, the mean exceeds the standard deviation, meaning the mean flow was reliably towards the southwest during this time. The 30 m plot (Figure 9a) shows these results graphically with a large variability at S2 through S5 with smaller standard deviations at S6 and S7. The deeper plot of 150 m (Figure 9b) shows the smallest standard deviation at the moorings over the slope.

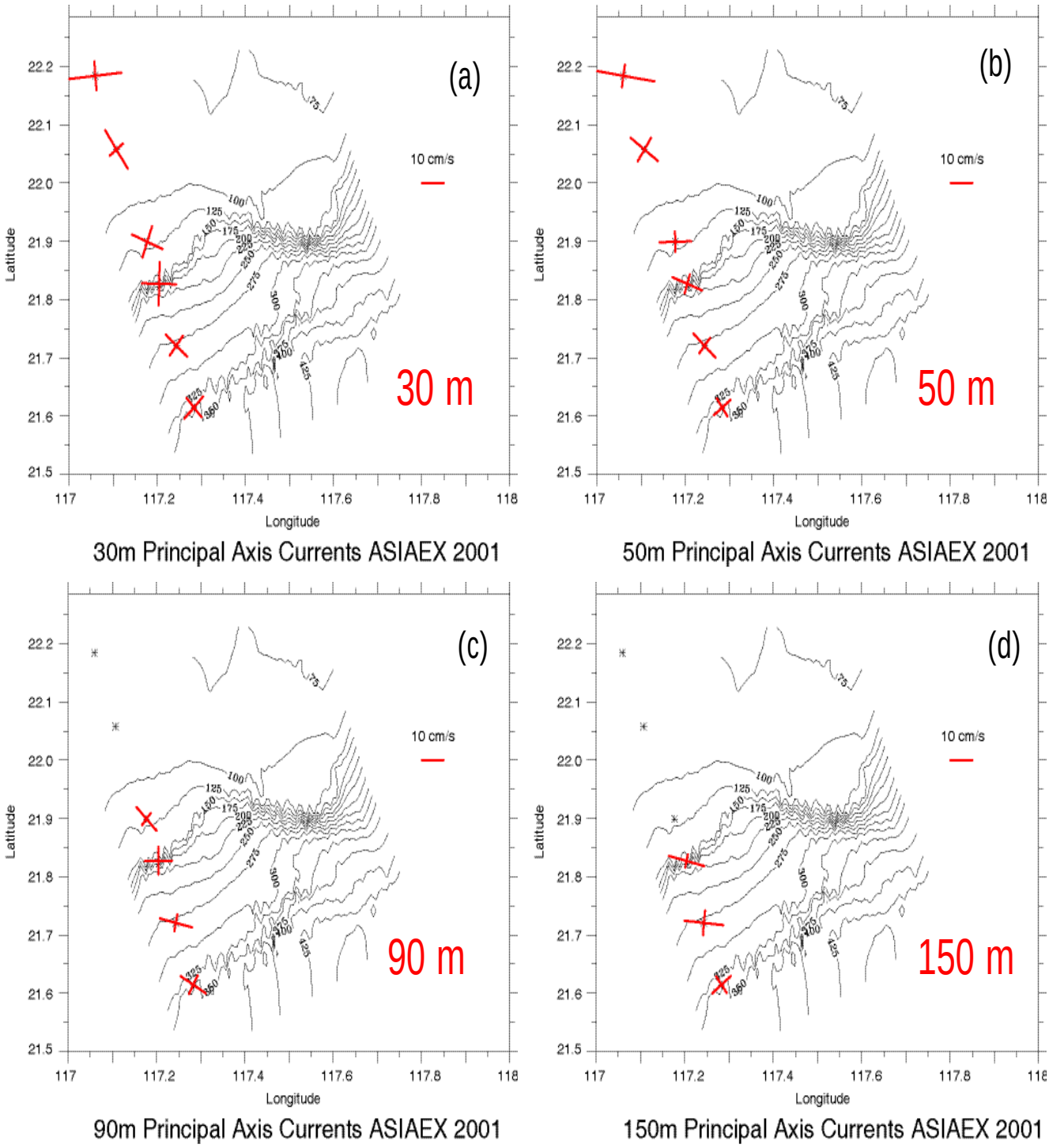

Figure 9. Principal axis map showing the standard deviation about the mean at each mooring, S2-S7. Depths of 30 m (a), 50 m (b), 90 m (c), and 150 m (d) are shown. The black solid lines are contour lines mapping the sea floor in the ASIAEX region.

B. TIME SERIES PLOTS

The time series plots show the temporal variability that was observed in the South China Sea during 21 April to 18 May 2001. During this short time period both significant wind forcing and multiple mesoscale events occurred. Observations included a possible appearance of the South China Sea Warm Current (SCSWC) at S6, energetic subsurface flows at S7, the passage of tropical cyclone Cimaron, and the possibility of the Kuroshio Intrusion extending into the ASIAEX area. Figure 11 shows the stick vector plots for all moorings at depths of 15 m, 50 m, and 100 m, with the coordinate system rotated 21 degrees counterclockwise to align with topography (Figure 10). Up in the figure represents the positive alongshore direction towards the northeast, and therefore a vector pointing downward and to the right represents an alongshore and slightly offshore flow towards the southwest. The winds at Dongsha (Pratis) Island, (Figure 11) were light and variable during this inter-monsoon period. Two periods of northeasterly wind during 21-26 April and 9-15 May were visually coherent with the surface currents. A major event can be seen at all moorings beginning on 9 May, apparently related to Cimaron which will be discussed subsequently. Surface currents over the shelf were deflected approximately 45 degrees to the right of the wind, consistent with Ekman dynamics. Flows at mooring S2 generally followed the sign of the wind stress. For the time period that S3 was working, it was also visually coherent with S2 and the wind stress. Mooring S4 contained mostly alongshore flow towards the southwest and did not follow the wind stress as well as S2 and S3 did. The time series at 15 m depth omits data for S5 and S6 because

results were not obtained this close to the surface due to surface side-lobe reflection. At 50 m and 100 m depth moorings over the slope (S5-S7) had flows towards the southwest which agreed with the mean vectors from Figure 8. Some variation occurred at these moorings which were related to the movement of the northern cyclonic gyre. Current magnitudes, ignoring the major event on 9 May, ranged from 15-17 cm/s at the surface, and 12-15 cm/s throughout the water column, decreasing in the bottom boundary layer. These figures give a good representation of the mesoscale variability along the entire ASIAEX area as well as throughout the water column. The time series depth at 100 m only shows results for S5, S6, and S7 because the others are too shallow and do not exist at this depth.

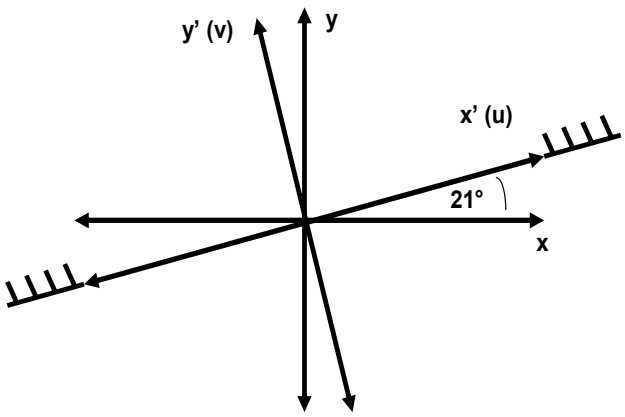

Figure 10. Rotation of the coordinate system 21° to align with topography. The small slanted lines represent the coast. The alongshore is now represented by u while the across-shore is represented by v.

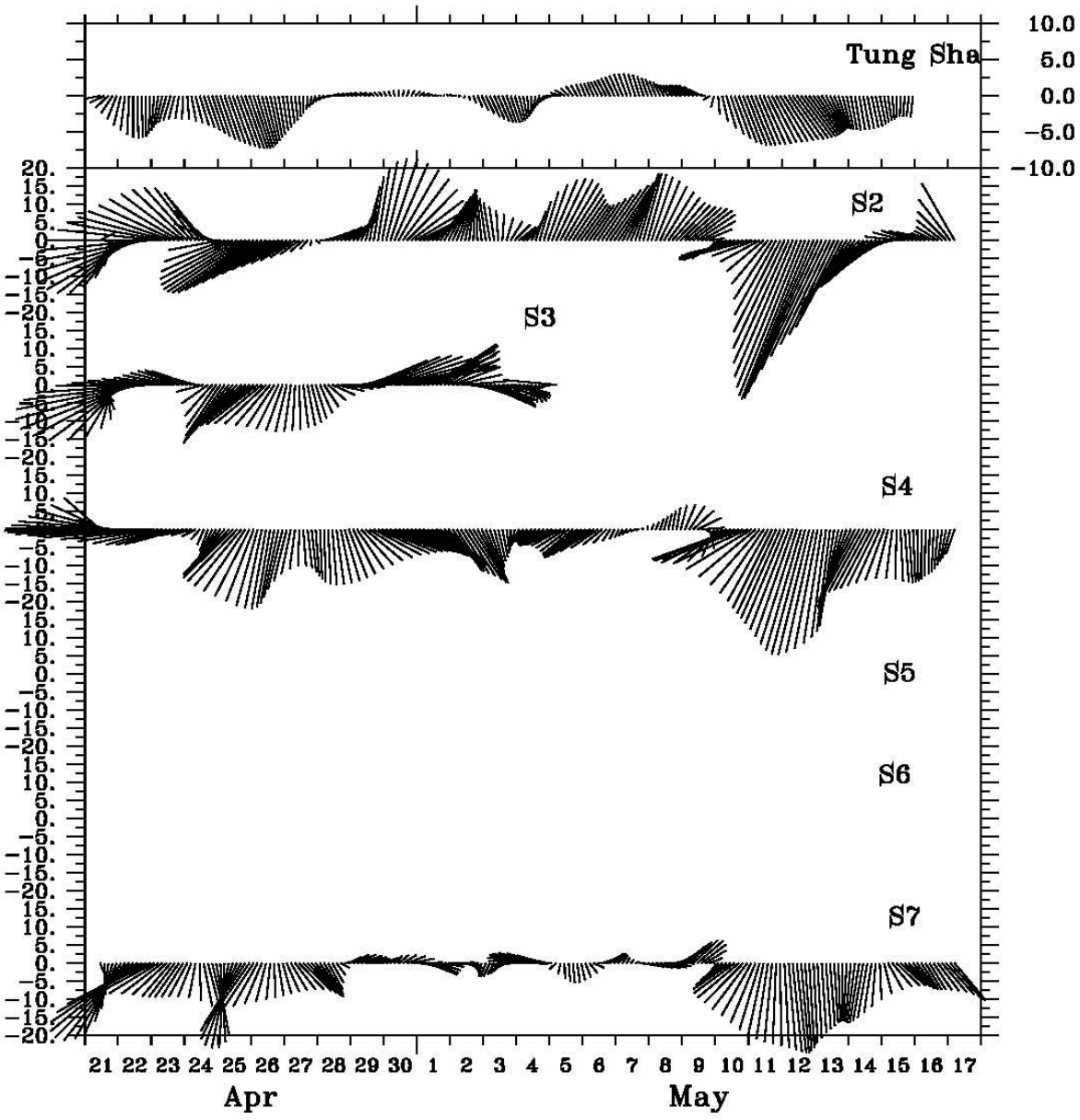
Tung Sha
S2
S3
S4
S5
S6
S7
10.0
5.0
0.0
-5.0
-10.0
21 22 23 24 25 26 27 28 29 30 1 2 3 4 5 6 7 8 9 10 11 12 13 14 15 16 17
Apr
May

15m

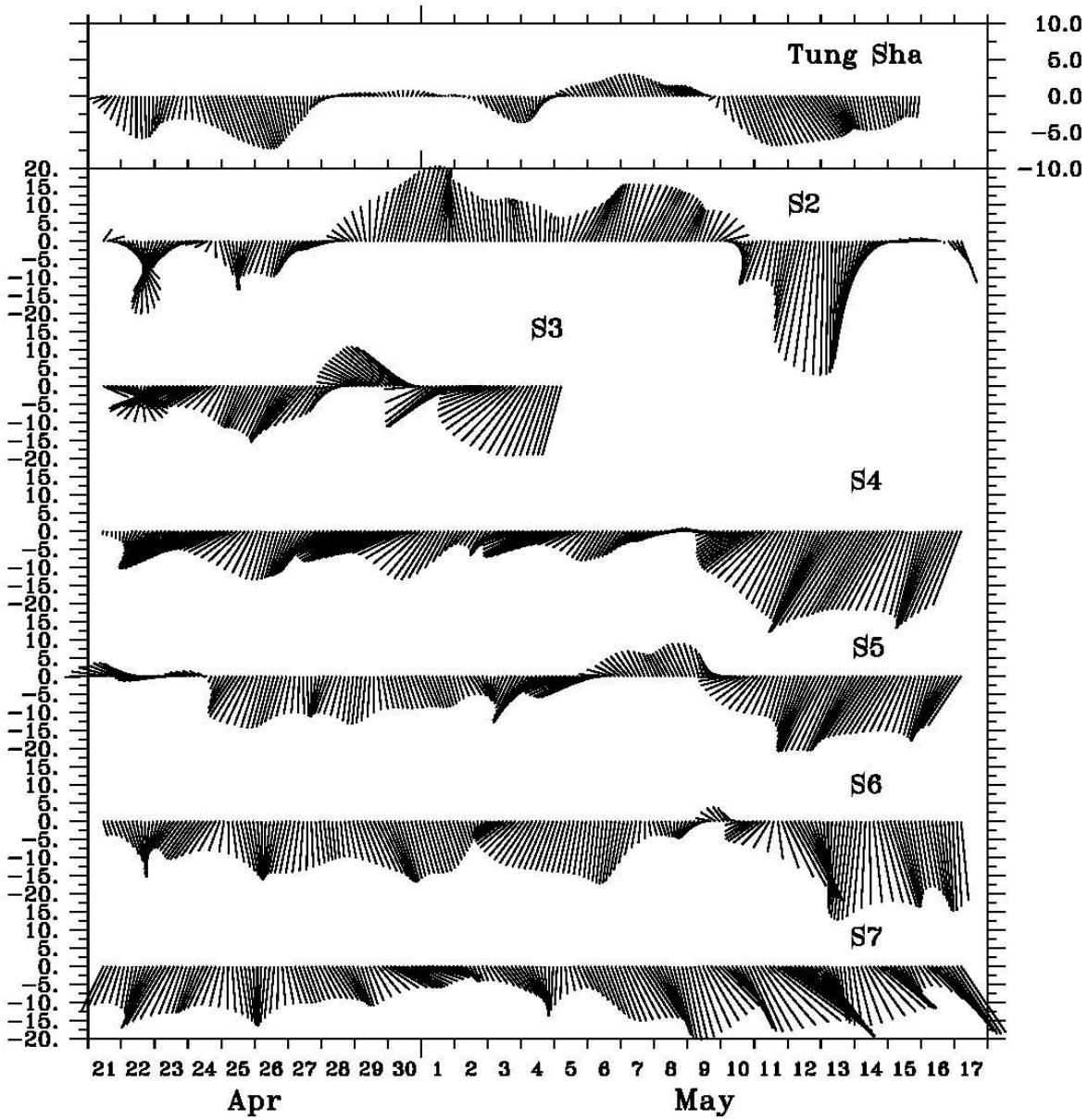
Tung Sha
10.0
5.0
0.0
−5.0
−10.0
S2
S3
S4
S5
S6
S7
20.
15.
10.
5.
0.
−5.
−10.
−15.
−20.
21 22 23 24 25 26 27 28 29 30 1 2 3 4 5 6 7 8 9 10 11 12 13 14 15 16 17
Apr
May

50m

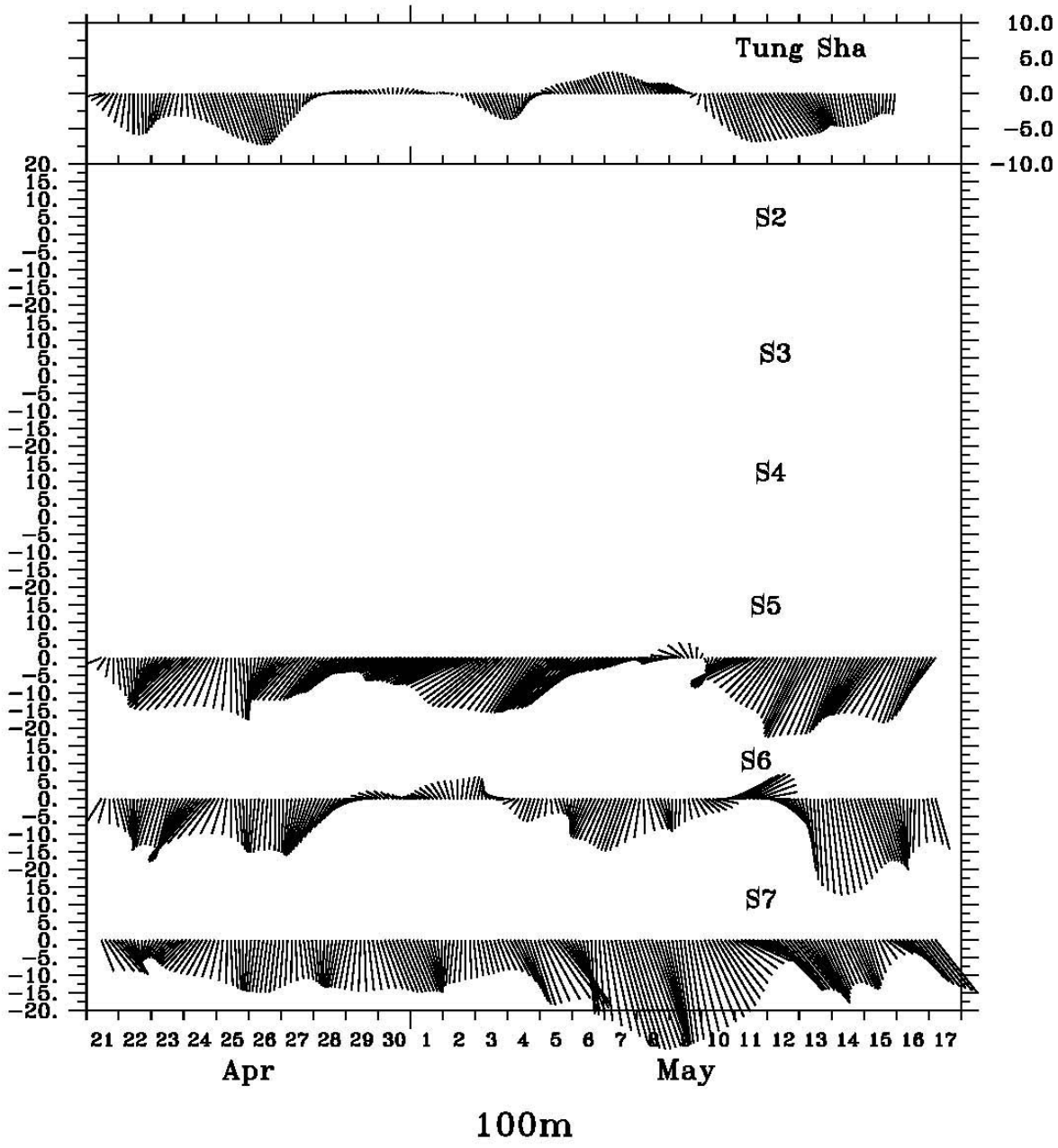

Figure 11. Stick vector plots of all moorings (S2-S7) at 15 m, 50 m, and 100 m. with the coordinate system rotated 21 degrees to align with topography. Up represents the positive northeast direction. The winds at Dongsha (Tung Sha) Island are plotted at the top of each figure.

C. CURRENT REVERSALS AT MOORING S6

Two interesting current reversals were observed at mooring S6 during the ASIAEX time series (Figures 11-15). The first appearance began on 1 May at 0800, reached a maximum reversal at 2000, and continued until 3 May at 1000. The second reversal can be seen on 11 May at 0900. The alongshore velocity component shows a subsurface northeastward flow at S6 below 100 m depth which is counter to the general southwestward flow. This flow reached a maximum velocity of 15 cm/s at mooring S6 only. This northeastward flow over the slope is consistent with what was previously named the South China Sea Warm Current (Chao et. al, 1994). The surrounding water at S5 and S7 continued to flow to the southwest at 5 to 10 cm/s. The cross-shore velocity contours show that at S5 flow was strongly onshore at > 20 cm/s while flow at S7 was weakly offshore at 5 cm/s (Figure 12). The strong southwestward current seemed to meander offshore until it only occurred at S7. These two flows produced divergence at S6 which allowed the South China Sea Warm Current to fill in from the south. The cross-shore component gives evidence that the divergence on 1 May was due mostly to the onshore flow at S5. Figure 13 shows a progression of the salinity contours during the reversal event on 1 May, which shows the subsurface salinity maximum as it retreated offshore. This maximum has a salinity of 34.7 and occurred at a depth of 150 m which suggests that the water retreating is a remnant of the Kuroshio Intrusion. As the salinity maximum of the Kuroshio Intrusion retreats offshore, the South China Sea Warm Current is able to enter from the south.

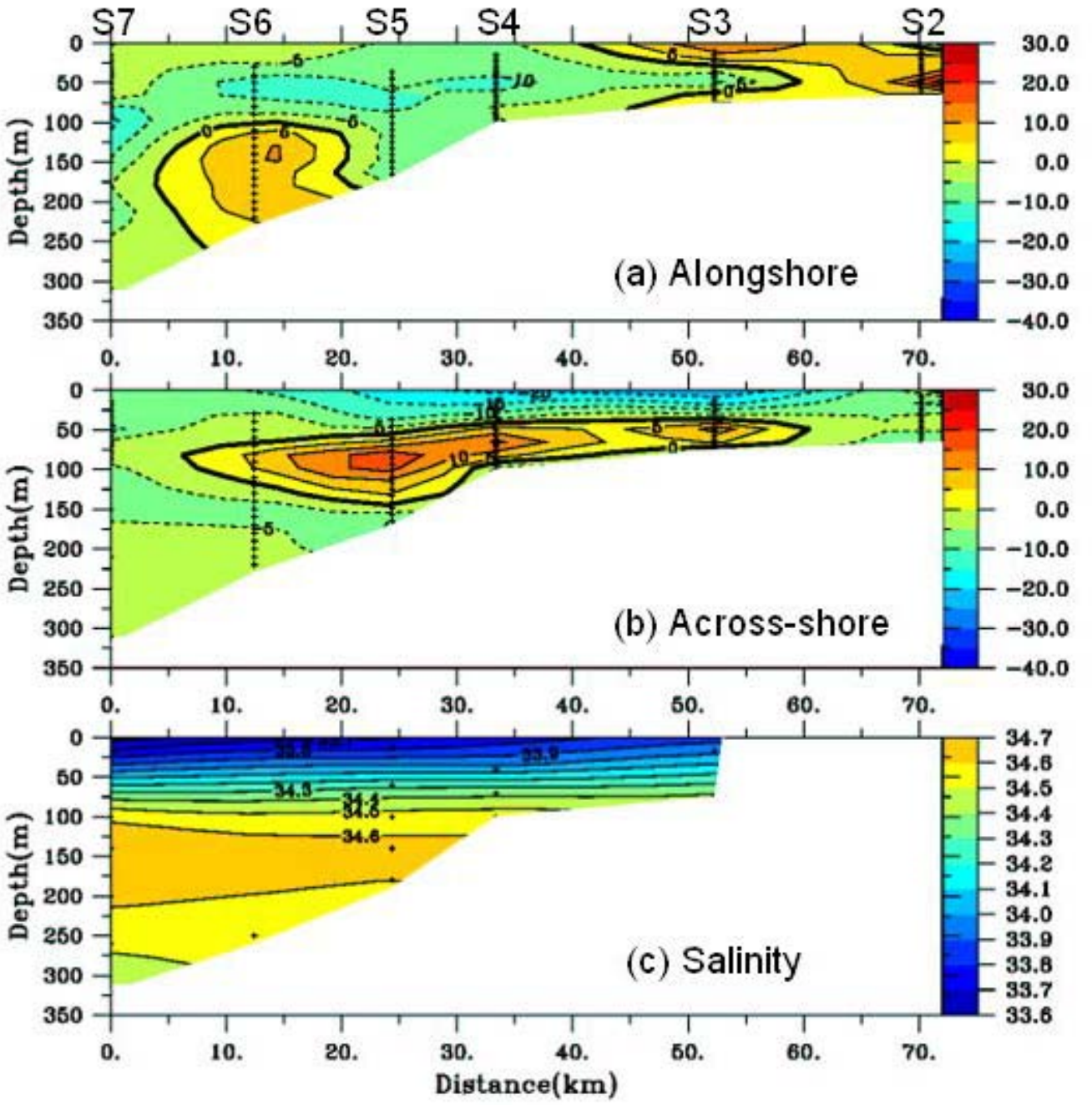

Figure 12. Contour plot of the flow reversal at S6, (12 km) on 1 May at 0800. (a) alongshore (u) flow (b) across-shore (v) flow, (c) salinity. The black crosses represent each mooring with S7 at the far left and S2 at the far right of the plot.

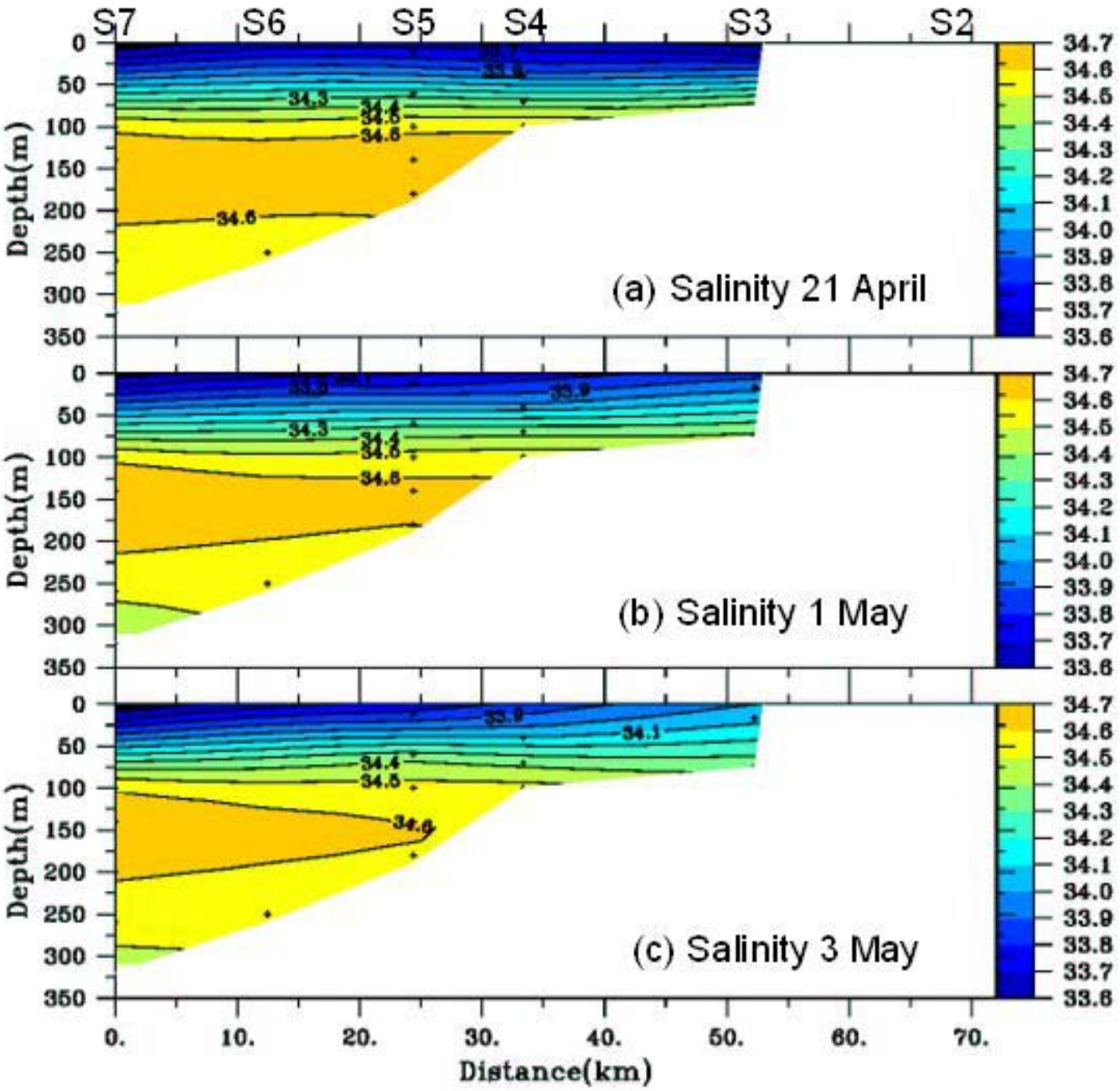

Figure 13. Salinity progression plots during the flow reversal at S6 on 1 May showing the retreat of the salinity maximum at 150 m depth. (a) 28 April 2001 at 2100, (b) 1 May 2001 at 0800, and (c) 3 May 2001 at 0600.

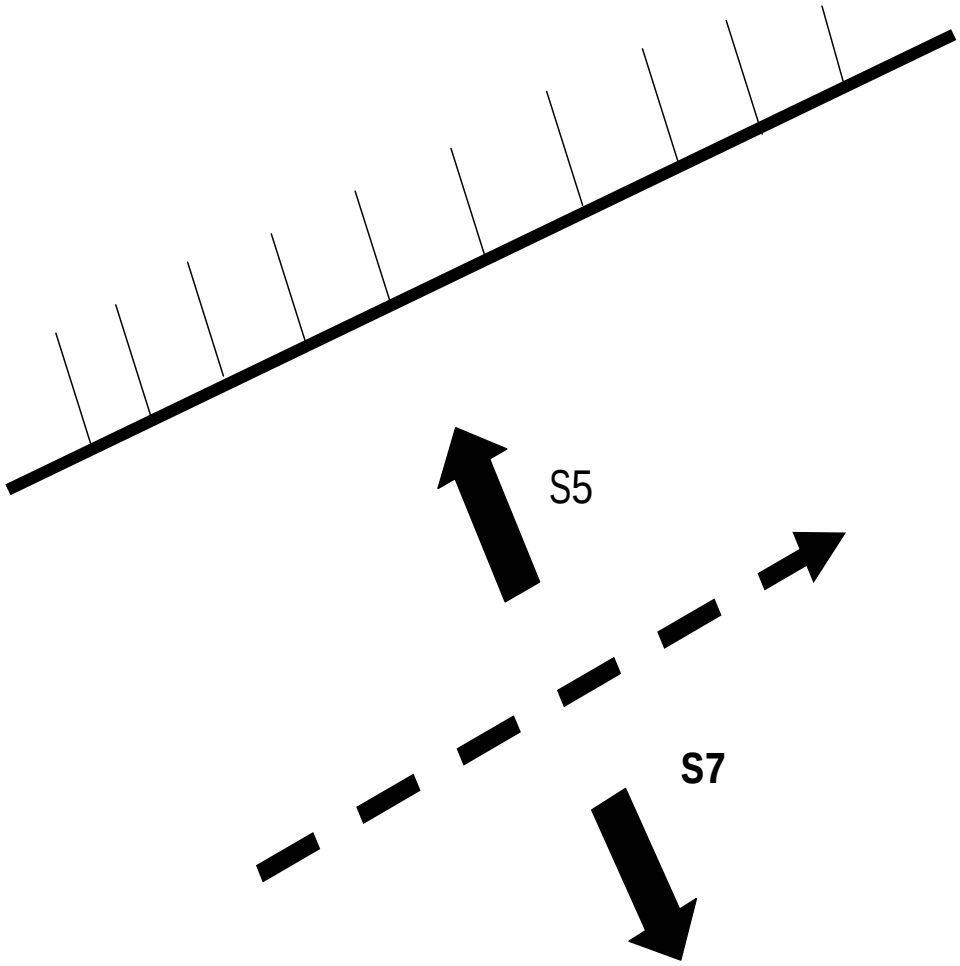

Figure 14. Cartoon figure of the South China Sea Warm Current to demonstrate the divergence between moorings S5 and S7

The weaker existence of the South China Sea Warm Current on 11 May can be seen in Figure 12 which shows the alongshore and across-shore contours as well as the salinity contours of the second flow reversal at S6. Although this reversal was less intense than the one that occurred on 1 May, it still demonstrated the South China Sea Warm Current's existence as a subsurface feature in the ASIAEX area. This weaker reversal only reached a velocity of 10 cm/s in the northeast direction with velocities ranging from 5-10 cm/s in the southwest direction at S5 and

S7. An onshore flow of >15 cm/s is still seen at mooring S5. Compared to the only slightly offshore flow at S7 during the first reversal, a stronger offshore flow of >10 cm/s was seen during this second event. Again these two flows produced divergence at S6 allowing for the South China Sea Warm Current to intrude from the south. The stronger offshore flow at S7 also caused more offshore movement of the mid-depth salinity maximum than during the first event.

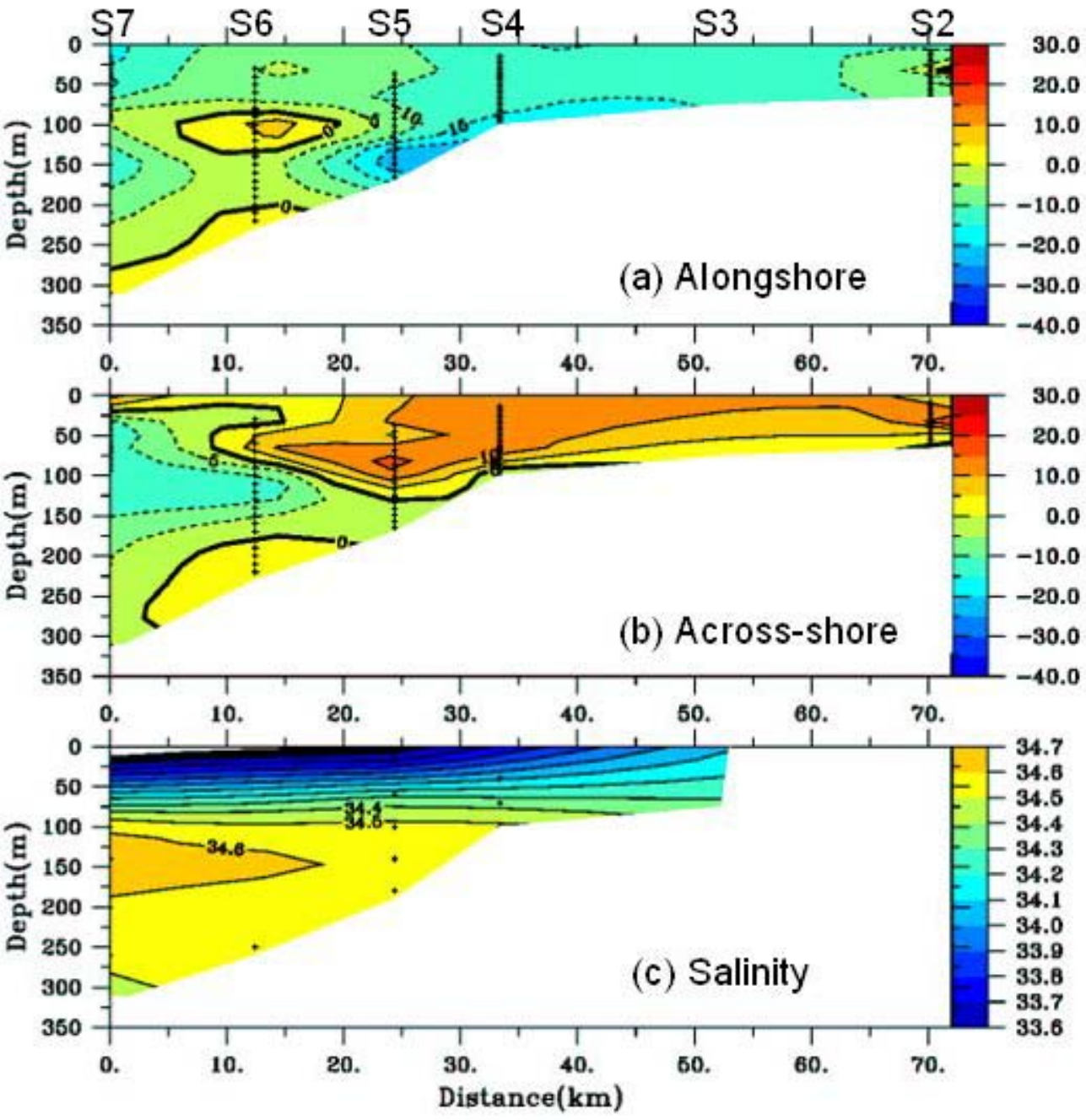

Figure 15. Contour plot of the flow reversal at S6, (12 km) on 11 May at 0900. (a) alongshore (u) flow (b) across-shore (v) flow, (c) salinity. The black crosses represent each mooring with S7 at the far left and S2 at the far right of the plot.

D. CYCLONIC MEANDER AT S7

Stick vector plots as a function of depth at S7 show a subsurface current between 3 and 9 May bringing energetic flows of up to 34 cm/s at depths from 59 m to 150 m (Figure 16). This feature was still present but slightly weaker at 210 m, and much weaker near the bottom (310 m). Analysis of the stick vector plots at S7, suggest that it could possibly be an eddy generated more offshore or the northern edge of a cyclonic meander propagating east to west past S7. The upper 30 meters of the water column saw weak flows to the southwest during this time, i.e., this was clearly a subsurface feature. As the time series progressed from 3 to 9 May, the stick vectors rotated from an onshore south southwestward flow to an alongshore southwestward flow. This progression from 3 to 9 May also saw a velocity increase from 10 cm/s to a maximum of 34 cm/s between 7 and 8 May. The eddy/cyclonic meander maintained intense flows through the water column until just above the seafloor, at 310 m depth. Here it was influenced by bottom topography, making it less intense along the sea floor interface. It should also be noted that the flows between 59 m and 150 m were remarkably steady during 5-9 May, with little to no variation in velocity. The direction of the flow slowly progressed from a slightly onshore flow to almost completely alongshore until on 10 May, the flow changed sharply to onshore as the feature passed by the mooring (Figure 16). This eddy/cyclonic meander was believed to have been formed in deeper water further offshore than the deepest mooring of the ASIAEX experiment, mooring S7. It appears that the eddy progressed onshore as a cyclonic flow that penetrated towards the northwest. It continued up to the continental shelf, until it felt the bottom and was

therefore forced to follow topography to the southwest. More specifics of the eddy/cyclonic meander will be discussed subsequently in the model/data comparison section.

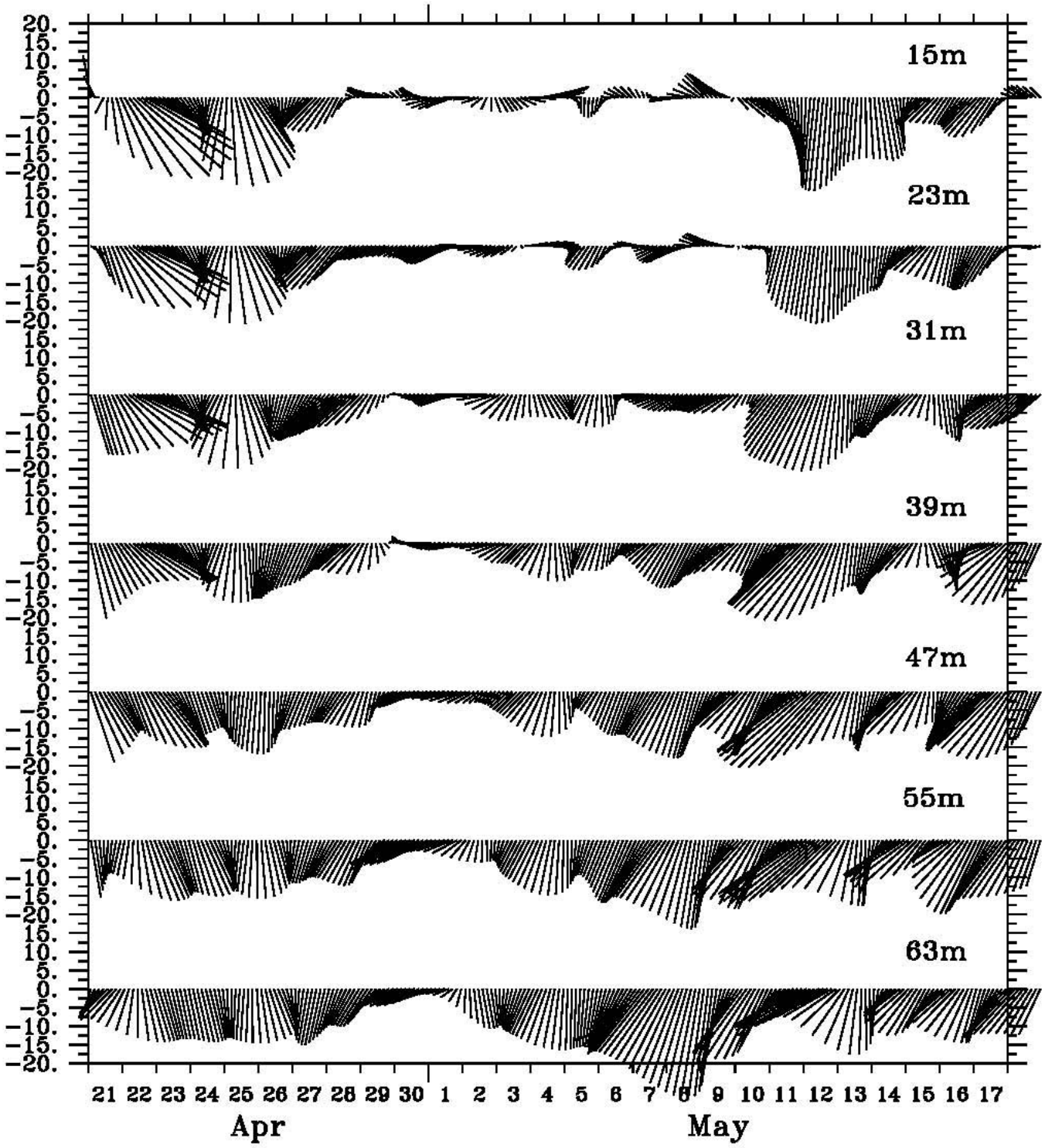
15m
23m
31m
39m
47m
55m
63m
21 22 23 24 25 26 27 28 29 30 1 2 3 4 5 6 7 8 9 10 11 12 13 14 15 16 17
Apr
May

S7

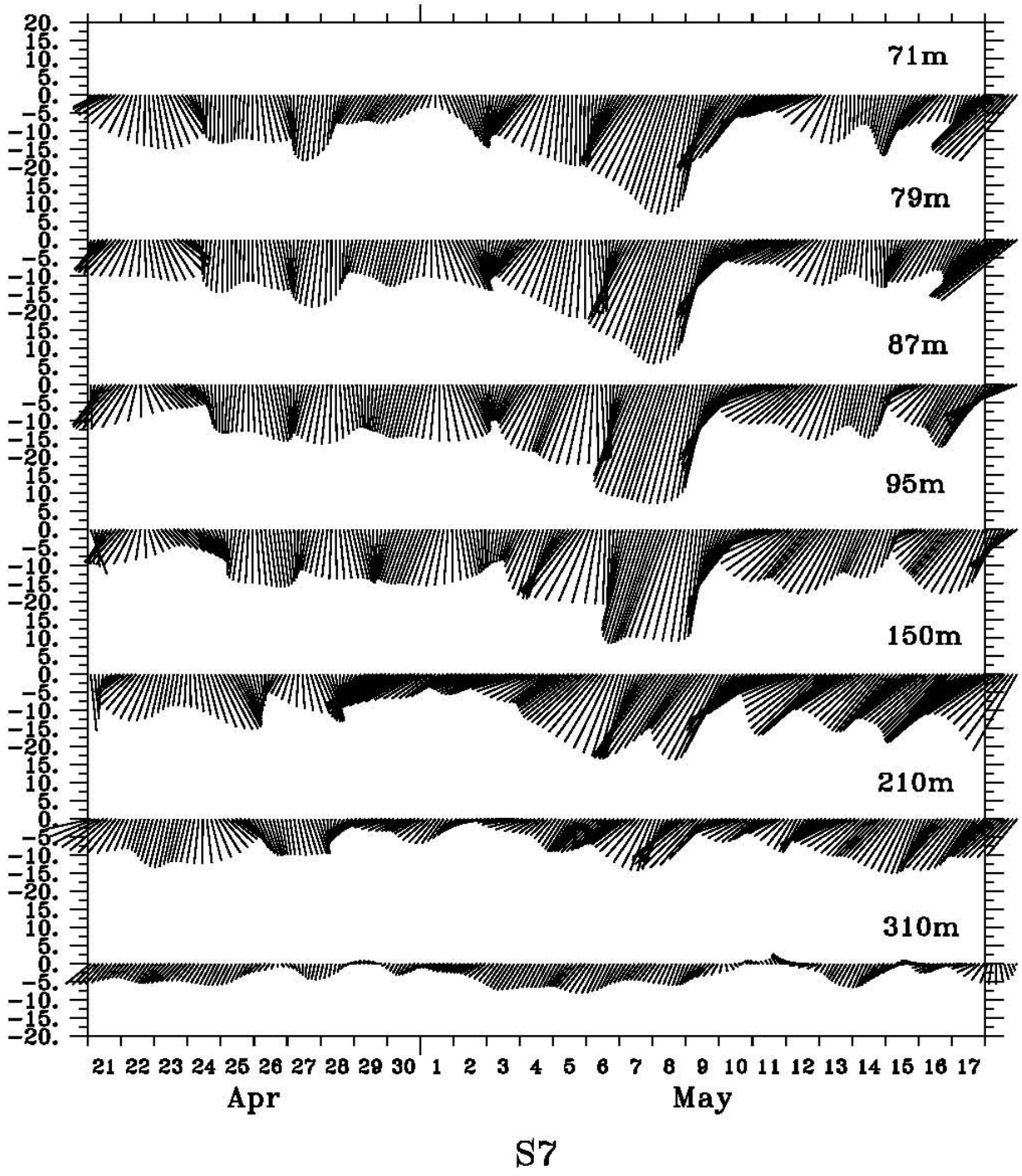

Figure 16. Current vector plots of mooring S7 from 15 m to 310 m depth. The coordinate system was rotated 21 degrees to align with topography and therefore up represents the positive northeast direction. The current vectors from 15-95 m are from the ADCP and at 150, 210, and 310 m from the Aanderra current meters.

E. IMPACT OF CYCLONE CIMARON

Tropical Cyclone Cimaron crossed the northern South China Sea on 13 May until it continued on its path out of the Luzon Strait and into the Philippine Sea (Figure 7). The satellite AVHRR visual-band image of Cimaron (Figure 7) shows that the storm covered the entire Luzon Straits region on 13 May 2001. In the ocean, constant intense flows of 47 cm/s were seen from 8 m to 32 m depth at ASIAEX shelf mooring S2 (Figure 17). At 32 m depth the current magnitude was still 37 cm/s and decreased only in the bottom boundary layer at 60 and 64 m depth (Figure 17). There was no evidence of vertical shear or turning of the current vector as a function of depth, as would usually be expected under forcing by the surface wind stress. The wind speed at Dongsha Island, only 10 m/s, was not strong enough to drive a 47 cm/s surface current. These results suggest these currents were down-gradient pressure driven flows rather than the result of Ekman dynamics. The size of this storm apparently elevated sea level in the western South China Sea via the inverse barometer effect. The resulting down-gradient flow was not geostrophic because it was constrained by topography (the Chinese coast) on the right. The feasibility of this hypothesis will be examined further using a quantitative calculation in the discussion section.

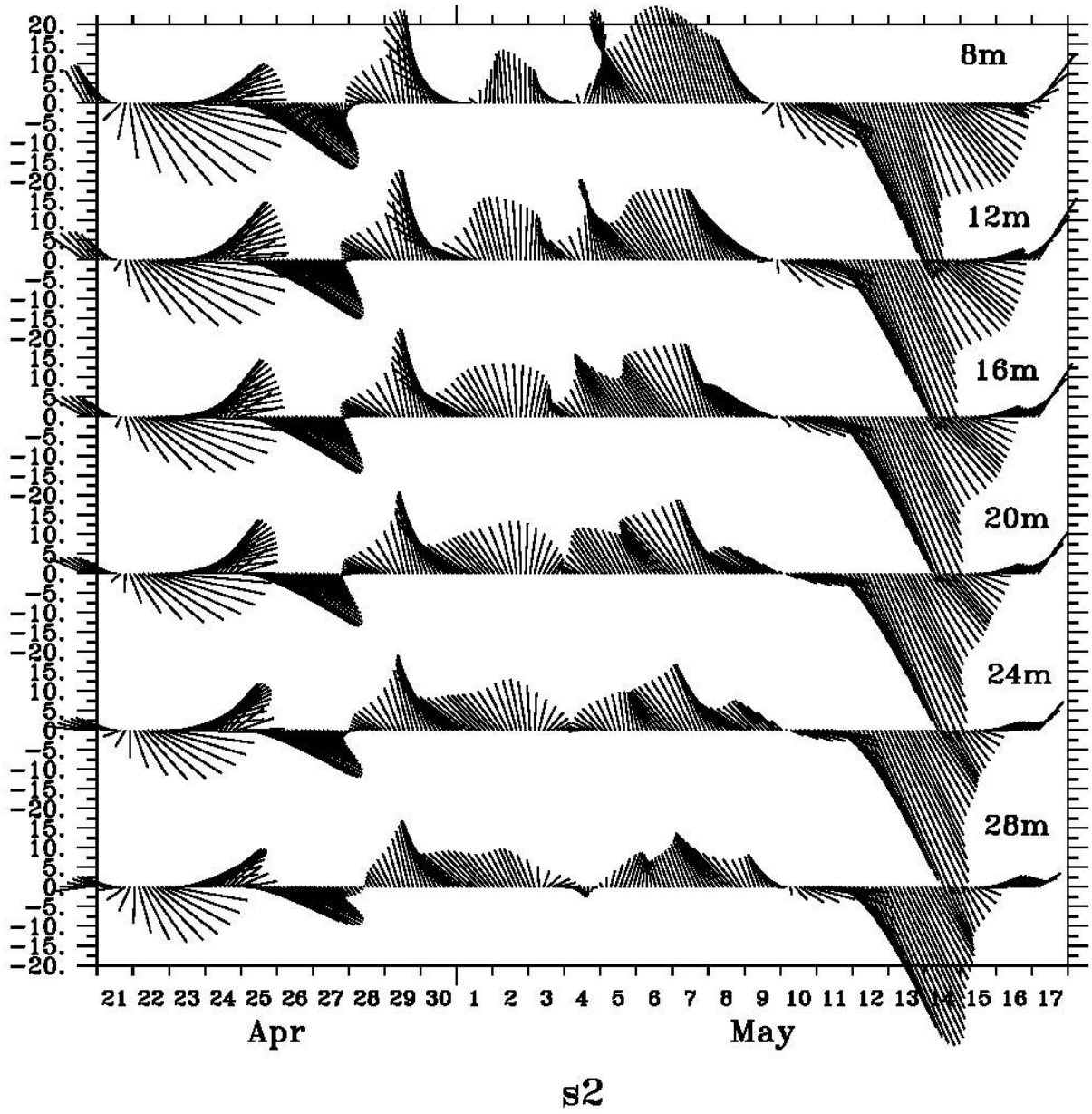
8m
12m
16m
20m
24m
28m
21 22 23 24 25 26 27 28 29 30 1 2 3 4 5 6 7 8 9 10 11 12 13 14 15 16 17
Apr
May

s2

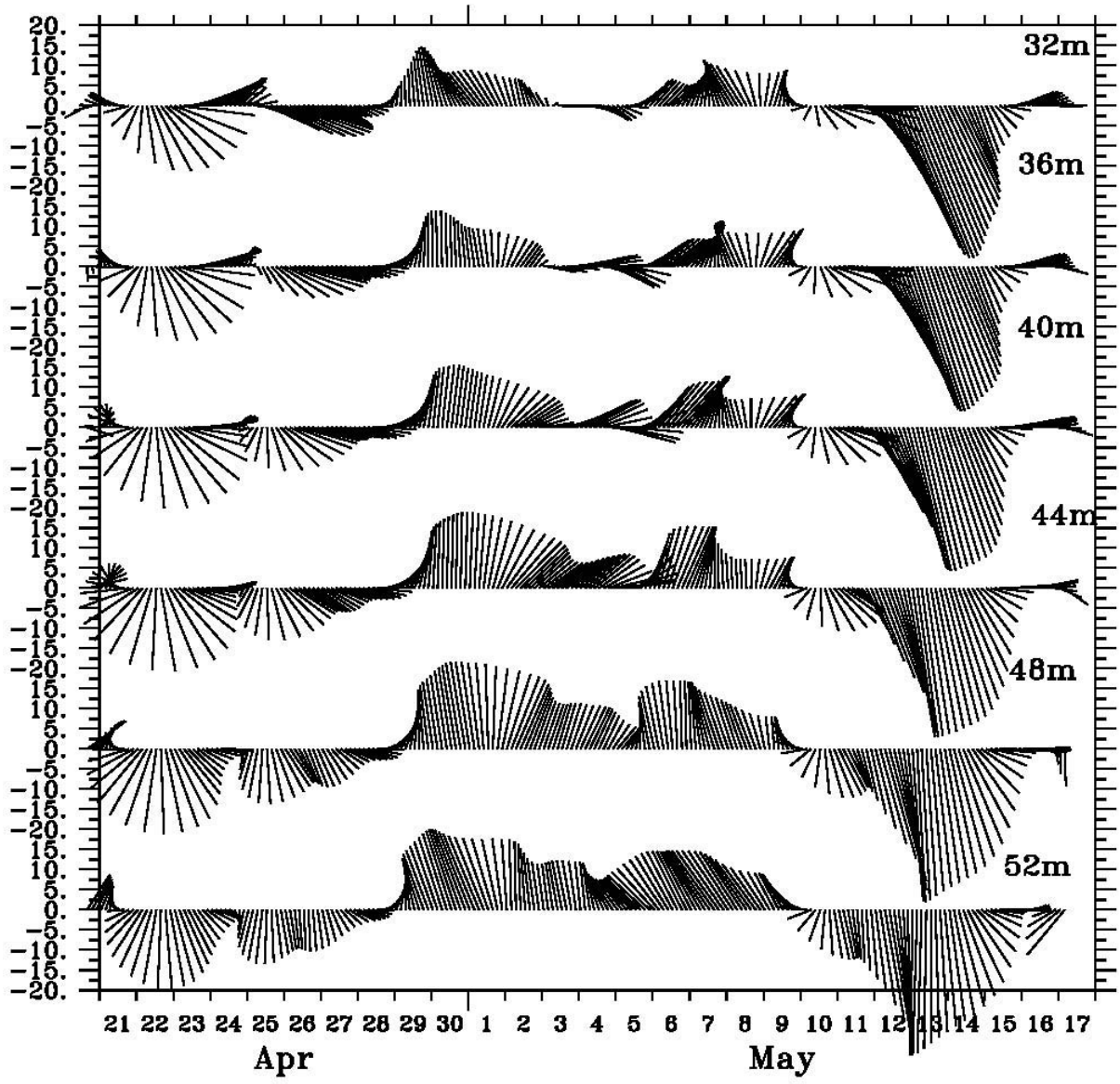
32m
36m
40m
44m
48m
52m
21 22 23 24 25 26 27 28 29 30 1 2 3 4 5 6 7 8 9 10 11 12 13 14 15 16 17
Apr
May

s2

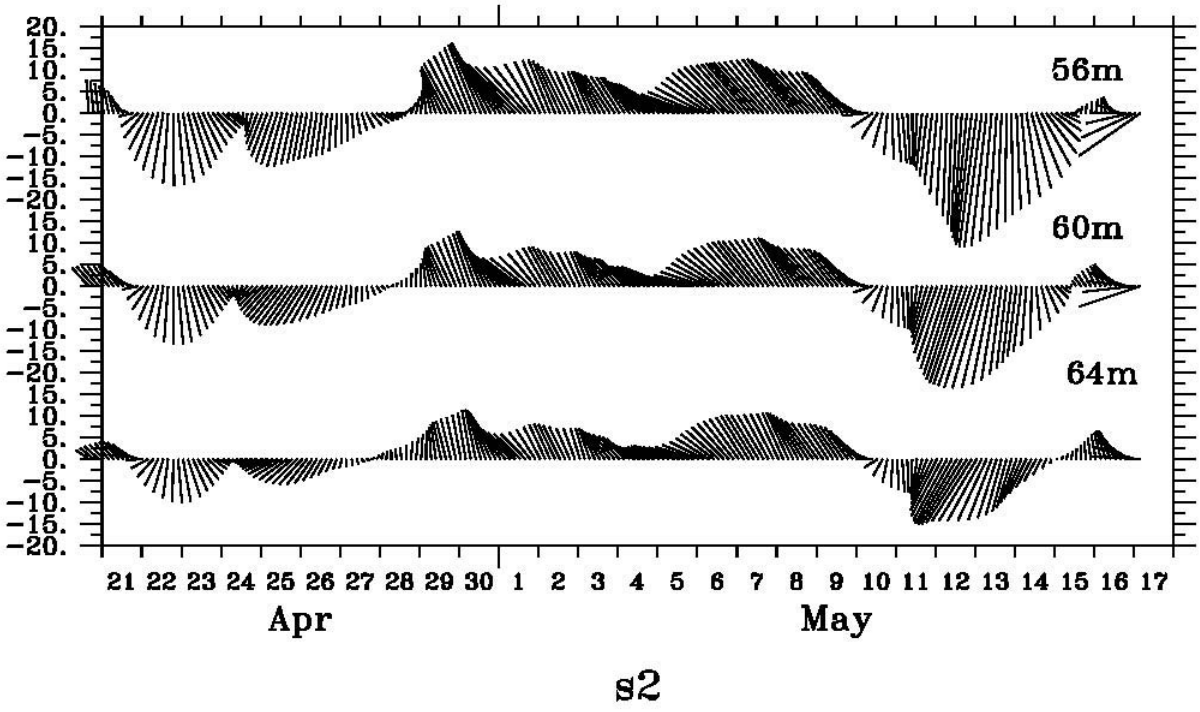

Figure 17. Current vector plots of mooring S2 from 8 m to 64 m depth. Like the previous stick vector plots the coordinate system was rotated 21 degrees to align with topography and therefore up represents the positive northeast direction.

F. AUTO AND CROSS SPECTRA / COHERENCE AND PHASE

Despite the short record length, spectral plots (not referenced here) were created to give some idea of the frequency dependence of wind and current at each mooring. Both the wind and currents over the shelf had a spectral peak at 7.5 days. The cross-spectra for S2 and S4 versus wind showed that over the shelf the currents were coherent with the wind stress at this period. This period is typical for continental shelf environments. The wind and currents were in phase at S2, and wind led current by 12 hours at deeper S4. Moorings S5, S6, and S7 were over the slope and therefore were not as affected by the local wind

throughout the water column. These moorings reach depths of up to 350 m which was too deep to allow for direct forcing by the wind. The phase lag between wind and current increased between S2 and S7, as deeper waters were approached.

IV. DISCUSSION

A. MODEL BACKGROUND

The Northern South China Sea Nowcast/Forecast System (NSCSNFS) is a high resolution, regional, numerical-model-based, real-time ocean prediction system for the northern South China Sea (Chapman et. al., 2004, Ko et. al., 2003a, 2003b; Wu, 2003; Hwang et. al, 2004; Lee, 2003). It is based on the 1/24° Princeton Ocean Model and contains 30 vertical layers. These layers are concentrated near the surface and bottom in order to resolve the boundary layers. Topography is fed into the model grid from a two-minute global topography database called NRL DBDB2. Open boundary sea surface heights, currents, temperatures, and salinities are provided by the North Pacific Ocean Nowcast/Forecast System (NPACNFS), a model similar to NSCSNFS but on a larger scale. The Navy Operational Global Atmospheric Prediction System (NOGAPS) provides surface forcing fields including wind stress, total heat flux, solar radiation, and sea level air pressure. Real time data including sea surface heights and mean current sea surface temperature (MCSST) are also assimilated into the model (Chapman et. al., 2004).

B. MODEL OUTPUT VS OBSERVATIONAL DATA

The model output was obtained from Dr. Dong-Shan Ko of the Naval Research Laboratory (NRL). Output was provided for each of the ASIAEX mooring locations at standard depths of 15, 45, 75, 100, 140, 180, 210, and 310 m. The velocity components were low-pass filtered with the same filter as the current meter data, and rotated into the same along- and across-shore coordinate system. The model output and

observational data were compared via visual graphics and statistical comparisons.

The fluctuations in the model alongshore currents over the continental shelf seemed to follow the observations except for a distinct offset of at least 20 cm/s at the surface and at 45 m depth (Figure 18). The reason for this offset can be linked to a persistent northeastward coastal current predicted by NSCSNFS which was not observed in the data. The mean and standard deviations of the differences between model output and observational data were calculated for both the alongshore and across-shore components (Table 2). The coastal current was persistent throughout the time series except when strong northerly wind events occurred. The northeastward coastal current in the NSCSNFS was imposed at the northern boundary of the Taiwan Strait by NPACNFS (Dong-Shan Ko-personal communication). NPACNFS is a larger scale model that NSCSNFS is nested within (Chapman et. al., 2004). There is a small possibility that the northeast coastal current could have been caused by a bias in the wind stress; or an inaccurate interpolation of wind stress, however it is more likely that is was imposed by NPACNFS (Dong Shan Ko- personal communication).

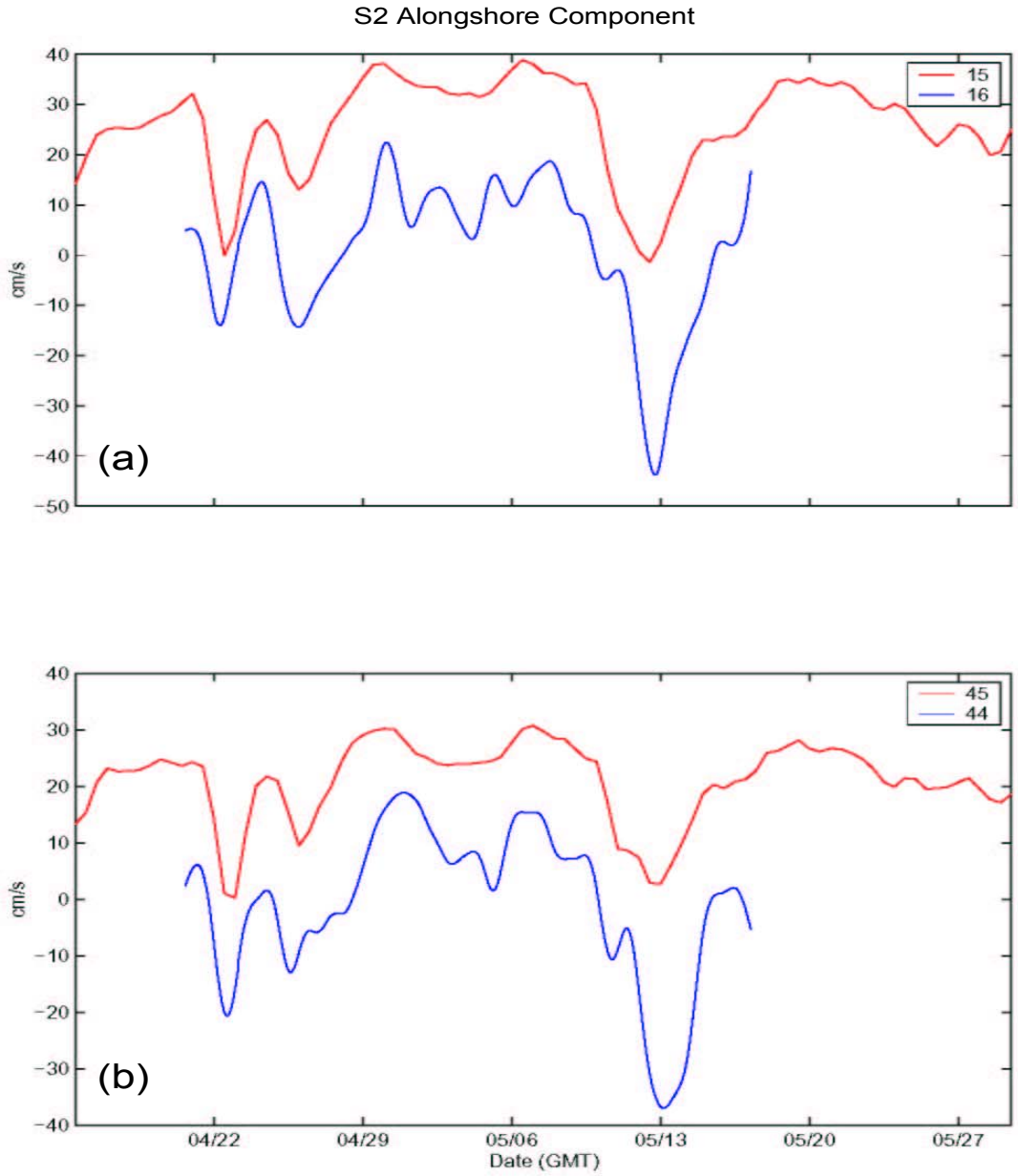

Figure 18. The alongshore component of velocity at S2. The red line represents model output while the blue line represents observational data. (a) at 15 and 16 m respectively; (b) at 45 and 44 m respectively.

	Model Depth	Observation Depth	Mean (u)	Standard Deviation (u)	Mean (v)	Standard Deviation (v)
S2	15	16	23.732	8.076	2.277	10.241
	45	44	20.837	7.943	-1.368	7.356
S4	15	14.5	12.342	7.872	-3.846	7.824
	45	46.5	14.006	5.657	-12.613	4.269
	75	74.5	14.803	5.958	-6.745	6.305
	100	98.5	8.208	5.956	3.969	5.127
S5	45	45	6.364	8.143	-9.855	5.764
	75	77	12.165	7.986	-14.647	6.984
	100	101	8.841	10.268	-11.814	5.776
	140	141	10.264	10.678	-1.263	5.121
S6	45	40	3.871	6.726	-6.24	5.634
	75	80	3.167	8.106	-6.567	6.039
	100	100	-2.013	8.998	-5.127	6.7
	140	140	-5.726	9.616	-2.301	5.892
	180	180	-8.529	7.561	-1.997	4.35
	210	210	-6.651	6.358	-1.265	3.07
S7	15	14.5	1.498	10.432	-0.709	9.549
	45	46.5	3.036	5.098	-0.975	7.982
	75	74.5	4.729	7.432	-1.678	6.97
	210	210	-0.287	3.693	0.882	4.836
	310	310	2.105	3.59	1.329	2.353

Table 2. The mean and standard deviations of the *differences* between model output and observational data for all moorings (S2-S7). Results for S3 were not computed due to its short data set.

The S2 and S3 alongshore component of the model closely resembles the observational data, capturing all major fluctuations throughout the time series (Figure 18). The across-shore component of the model currents did not compare as well as the alongshore component. The model seems too constrained to follow topography when there are in fact large across-shore flows present. The best example of this can be seen in Figure 19 which shows the across-shore flows at S5. The model output does not at all

resemble the observational data. It seems the model is too constrained, that it is forcing the water to follow topography at all depths and not just at deeper depths where the water is directly affected by topography. The mean differences exceed 10 cm/s between 45-100 m at S5 (Table 2).

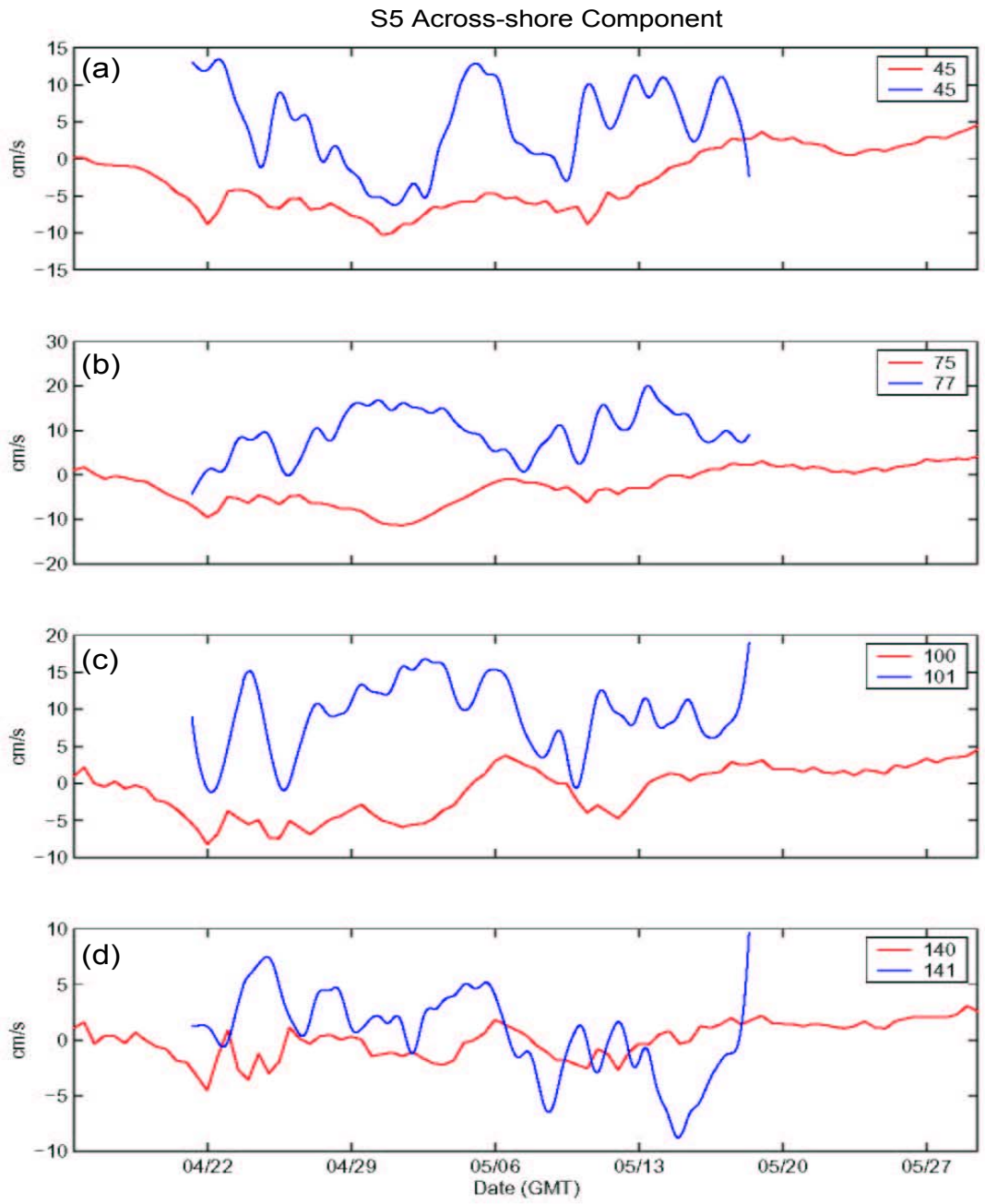

Figure 19. The across-shore component at S5. The red line represents model output while the blue line represents observational data. (a) at 45 m, (b) at 75 and 77 m respectively, (c) at 100 and 101 m respectively, and (d) at 140 and 141 m respectively.

The model also did not pick up two important features that were clear in the observational data. The observational data at mooring S6 show two distinct flow reversals which were previously determined to be the South China Sea Warm Current (Figures 12 and 15). The reversals were subsurface features that occurred below 100 m depth and were due to divergence produced by onshore flow at S5 and offshore flow at S7. As can be seen in Figure 20, the model does not resolve this subsurface, presumably pressure driven flow. Instead the model reveals a more or less constant flow to the southwest. This constant flow to the southwest occurred as the northern cyclonic gyre spread northward, turning water flow that was primarily onshore to alongshore flow to the southwest at the mooring line (Chapman et. al., 2004). A small Kuroshio Intrusion existed at this time but not enough to influence the flow to the southwest like the large scale eddy did. The failure of the model to produce the SCSWC may also be related to the incorrect across-shore flow at S5, since the correct model divergence is presumably necessary to simulate the flow.

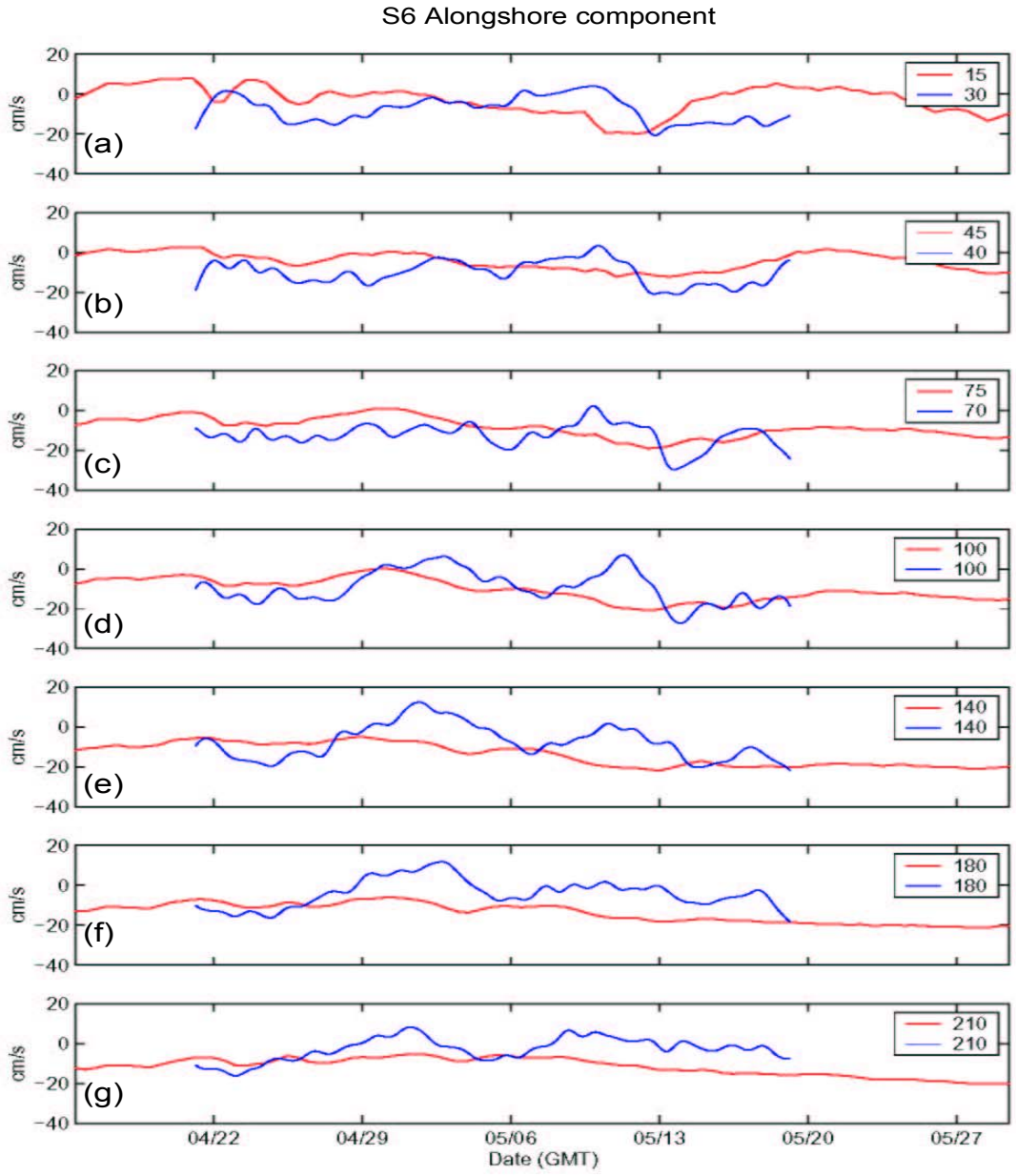

Figure 20. Alongshore velocity components at Mooring S6 versus model output. (a) 15 and 30 m respectively, (b) 45 and 40 m respectively, (c) 75 and 70 m respectively, (d) 100 m (e) 140 m, (f) 180 m, (g) 210 m

The eddy/cyclonic meander at S7, previously mentioned in this paper, appeared in the model data solely as a cyclonic meander as can be seen in the single snapshot of model output (Figure 21). It was not an eddy in the model as it never became fully enclosed but remained open on the southwest side. The NSCSNFS model showed the cyclonic meander propagating to the west and increasing in intensity with depth. The cyclonic meander seemed to pull away from the basin scale cyclonic gyre as it moved northward during the transition period. As it pulled away it brought fresher water into the ASIAEX area which eventually replaced the residual Kuroshio Intrusion water at slope (Dong-Shan Ko – personal communication). Another disagreement between model and observational data was that the onshore flow in the meander overshot isobaths in the observational data, while in the model data flow turned sharply and followed the isobaths. Besides this event, the model has much better agreement with observational data at S7 than at the other moorings. This is probably due to the flow at S7 following topography more closely than the other moorings. As a result the model output agrees with observational data better in deeper water.

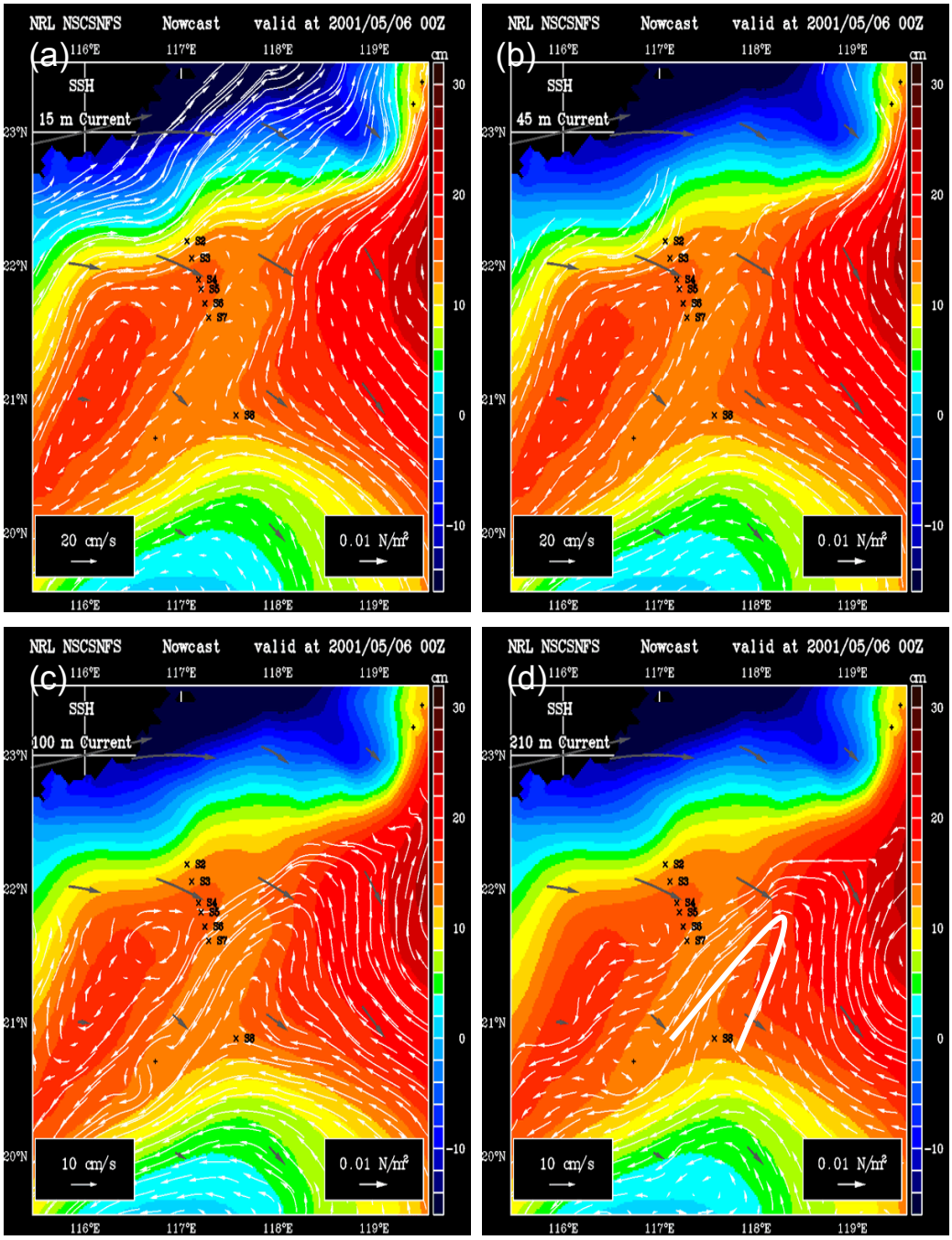

Figure 21. The Northern South China Sea Nowcast/Forecast System (NSCSNFS) output for (a) 15 m; (b) 45 m; (c) 100 m; (d) 210 m. The salinity scale is on the right in psu. The white arrow represents a scale velocity of 10 cm/s and the black arrows represent NOGAPS wind. The bold white line indicates the location of the meander feature (From: Dr. Dong-Shan Ko-personal correspondence)

C. FORCING BY TROPICAL CYCLONE CIMARON

The ASIAEX moorings show a new method of shelf/slope forcing due to the passage of a large tropical cyclone nearby. On 13 May Cyclone Cimaron was present in the South China Sea as can be seen by the current meter observations data but is less obvious in the model output. The model does catch the effects of the cyclone minimally at the surface, but fails to see the response at all at depth. The barotropic response suggests that the flow produced by the cyclone was primarily pressure driven. The low cyclonic pressure system of Cimaron set up the sea via the inverse barometer effect. This effect produced higher sea levels in the Luzon Strait than in the western SCS and therefore drove the along-shelf down-gradient flow to the southwest. The flow produced by Cimaron in the ASIAEX region was a remotely-forced barotropic flow, and did not look anything like the usual vertical sheared, locally wind driven flow (Figure 17).

A simple calculation was performed to test the feasibility that the currents due to Cimarron were primarily pressure driven. For a steady pressure driven flow to exist there must be a balance between the pressure force caused by the surface slope and the bottom stress (Ramp and Abbott, 1998). The bottom stress (τ_y^b) is also assumed to equal the surface stress (τ_y^s)

$$\tau_y^s = \tau_y^b = \rho C_d \upsilon_b^2 \qquad (1)$$

where ρ = density, C_d is the drag coefficient, and υ_b is the bottom velocity. The bottom drag coefficient (C_d) is

only an approximation as it does not account for tidal stress or stress due to surface wave motions interacting with the bottom, but only accounts for a balance with the surface stress (Grant et. al., 1984). For determining pressure driven flow in the South China Sea, a value of 10 x 10^{-3} will be used forced in accordance with the assumptions made in Ramp and Abbott (1998). The balance for steady pressure driven flow is given by

$$-c^2\left(\frac{\partial\zeta}{\partial y}\right)=B_y=\frac{\tau_y^b}{\rho} \qquad (2)$$

where c is the free wave speed, ζ is the surface elevation, and the other variables are as previously defined. Dividing by the water depth (H) and using $c^2=gH$, equation (2) becomes

$$\left(\frac{\partial\zeta}{\partial y}\right)=-\frac{\tau_y^b}{\rho gH} \qquad (3)$$

(Ramp and Abbott, 1998). As seen in Figure 17 of the velocity stick vector plots with depth the Cimaron current at the surface (υ_s) is 45 cm/s while the currents produced at the bottom (υ_b) = 17 cm/s. For ASIAEX, values of ρ = 1 g/cm^3, and C_d = 10^{-3}, g = 9.8 m/s^2 were used. Substituting into equation (2), a bottom stress (τ_b) of 2.89 g/cm^2 is obtained. Using this bottom stress and substituting into Equation (3) with H = 7200 cm a value of 4.1x10^{-7} is obtained for the surface slope.

The following equation was used to determine the surface elevation change needed below Cimaron to produce these currents

$$slope = \frac{\partial H}{\partial L} \qquad (4)$$

Using equation (4) and a distance (L) of 385 km to the Luzon Strait, an elevation of 15.8 cm was found. This value is a reasonable value resulting from a tropical cyclone. The meteorological record shows that the actual minimum surface pressures under Cimaron were commonly around 990 mb vs. an ambient atmospheric pressure of 1020 mb. Using the rule of thumb that 1 mb of atmospheric pressure deficit is equivalent to 1 cm of sea surface height elevation, the calculated value of 15 cm seems conservative. If the actual observed value of 30 cm were used, a higher value for the assumed drag coefficient is indicated, or perhaps a more gradual sea surface slope that extends beyond the ASIAEX line to the western South China Sea.

In order to check the above computations, the surface slope can also be estimated from the acceleration during wind relaxations in the upper segment of the water column (Ramp and Abbot, 1998).

$$\frac{\partial \zeta}{\partial y} = -\frac{\upsilon}{gt} \qquad (5)$$

Using a surface velocity (υ_s) of 45 cm/s yields a surface slope of 4.2 x 10^{-7}. Compared to the previous computation

of 4.1×10^{-7} these values are extremely close and therefore give confidence that the flow was pressure driven.

Model output from NSCSNFS agrees with the observations when looking at the basin scale circulation but is unable to resolve the South China Sea Warm Current. The model struggled particularly with the across-shore component over the shelf and slope, where model/data comparisons were poor. The overall model/data performance is summarized in Table 2. The coarse agreement between model and observations lets the big picture be seen and is therefore a good representation of the gyre-scale circulation in the South China Sea.

V. CONCLUSIONS

ASIAEX 2001 provided considerable insight into the coastal and mesoscale variability in the South China Sea. The experiment had a limited time series considering it only lasted from 21 April to 17 May. A longer data record would solidify results from this time series and would increase the confidence in the statistics presented in this thesis. Further research is currently going on in the South China Sea with the launch of the Windy Islands Soliton Experiment (WISE) 2005. This experiment will collect data for a year and will therefore be able to provide more information about the South China Sea, including data during all four seasons.

Analysis of the current meter data records in the ASIAEX area showed that significant mesoscale features exist in the South China Sea. Mean currents over the continental shelf were found to be primarily wind driven while flows over the continental slope were associated with the circulation offshore. The existence of the South China Sea Warm Current over the slope was observed twice during ASIAEX. This subsurface northeasterward flowing current was a direct result of across-slope divergence occurring between S5 and S7. A cyclonic meander was observed propagating through S7. This feature propagated on shore from deeper waters until it was steered by topography and then turned southwest in an along-shore path. The presence of Tropical Cyclone Cimaron to the east set up pressure driven flow towards the southwest along the continental shelf, suggesting that a storm this size can influence the circulation in the entire South China Sea.

Model results from the NSCSNFS were compared to the observational data. The model gave a good description of the gyre-scale circulation in the South China Sea but was unable to properly represent the South China Sea Warm Current or the forcing by tropical cyclone Cimaron. The model had a distinct offset of the alongshore component most likely brought on by open boundary forcing obtained from a larger scale model, the NPACNFS. The model was also too constrained by topography, forcing the water to follow topography at all depths and not allowing across-shore flow at mid-depth as observed. Although the model has room for improvement, it does give a good idea of the major flows in the South China Sea. The model allowed improved interpretation of a subsurface feature as a propagating meander rather than as a closed eddy.

The ASIAEX region crossed one of the primary sea lanes of communication between Chinese submarine bases and the Pacific theater. It is therefore considered a high priority region for naval research as tensions between China and Taiwan continue to exist. An improved understanding of the ocean circulation, density structure, and sound speed of the South China Sea will aid U.S. forces in safely navigating these waters if a crisis does arise. Knowing subtidal events will also improve the Navy’s ability to detect and prosecute enemy submarines as decision aids can now be constructed with the information gathered during ASIAEX.

LIST OF REFERENCES

Beardsley, R.C., T.F. Duda, J.F. Lynch, S.R. Ramp, J.D. Irish, C.-S. Chiu, T.Y. Tang and Y.J. Yang, 2004: The barotropic Tide in the Northeast South China Sea. IEEE J. Oceanic Engineering., vol. **29**, 1144-1156.

Broecker, W.S., W.C. Patzert, J.R. Toggweiler, and M. Stuiver, 1986: Hydrography, chemistry, and radioisotopes in the Southeast Asian basins, Journal of Geophysical Research, **91**, 14,345-14,354.

Centurioni, L.R., P.P. Niiler, and D.-K. Lee, 2004: Observations of Inflow of Philippine Sea Surface Water into the South China Sea through the Luzon Strait, American Meteorologica Society, **34**, 113-121.

Chao, S,-Y., P.-T. Shaw, and J. Wang, 1994: Wind relaxation as a possible cause of the South China Sea Warm Current, Journal of Oceanography, **51**, 111-132.

Chao, S.-Y., P.-T. Shaw, and S.Y. Wu, 1996: Deep water ventilation in the South China Sea, Deep-Sea Research I, **43**, 445-466.

Chapman, D.C., D.-S. Ko, and R.H. Preller, 2004: A high-resolution numerical modeling study of the subtidal circulation in the Northern South China Sea, IEEE J. Oceanic Engineering, **29**, 1087-1104.

Denbo, D.W., K. Lolain, J.S. Allen, A. Huyer, and R.L. Smith, 1984: Current meter observations over the continental shelf off Oregon and California February 1981-January 1984. Data Rep. 112, Ref. 844-12, College of Oceanography, Oregon State univ., Corvallis, OR.

Grant, W.D., Williams III, A.J., Glenn, S.M., 1984: Bottom stress estimates and their prediction on the northern California continental shelf during CODE-1: the importance of wave-current interaction. Journal of Physical Oceanography **14**, 108-112.

Hwang, C., C. Wu, and R. Kao, 2004: TOPEX/Poseidon observations of mesoscale eddies over the Subtropical Countercurrent: Kinematic characteristics of an anticyclonic eddy and a cyclonic eddy, J. Geophys. Res., 109, C08013, doi:10.1029/2003JC002026.

Ko, D.S., R.H. Preller, G.A. Jacobs, T.Y. Tang and S.F. Lin, 2003a: Transport Reversals at Taiwan Strait during October and November, 1999, J. Geophys. Res., 108(C11), 3370, doi:10.1029//2003JC001836.

Ko, D.S., R.H. Preller, and P.J. Martin, 2003: An Experimental Real-Time Intra Americas Sea Ocean Nowcase/Forecast System for Coastal Prediction, Proceedings, AMS 5th Conference on Coastal Atmospheric & Oceanic Prediction & Processes.

Lee, I.-H., 2003: Meso-scale Eddies in the Western Pacific and Their Influences on the Kuroshio, Ph.D. dissertation, National Taiwan University, pp 99.

Metzger, R.J., and H.E., Hurlburt, 1996: Coupled dynamics of the South China Sea, the Sulu Sea, and Pacific Ocean. J. Geophys. Res., **101**, 12,331-12,353.

Ramp, S.R., and C.L. Abbott, 1998: The vertical structure of currents over the Continental Shelf off Point Sur, CA, during Spring 1990, Deep-Sea Research II, **45**, 1443-1470.

Ramp, S.R., T.Y. Tang, T.F. Duda, J.F. Lynch, A.K. Liu, C.-S. Chiu, F. L. Bahr, H.-R. Kim, and Y.-J. Yang, 2004: Internal Solitons in the Northeastern South China Sea Part 1: Sources and Deep Water Propagation, IEEE J. Oceanic Engineering, **29**, 1157-1181.

Shaw, P.-T. and S.-Y. Chao, 1994: Surface circulation in the South China Sea, Deep-Sea Research I, **41**, 1663-1683.

Su, J., 1998: Circulation dynamics of the China Seas north of 18°N, Coastal Segment (12,S), The Sea, **11**, 483-505.

Wu, X., 2003: Assessment of A North Pacific Data-Assimilating Ocean Circulation Model as a Means for Downscaling to a High-Resolution, Extended Princes William Sound Circulation Model, Master thesis, RSMAS, University of Miami, pp 102.

Wyrtki, K., 1961: Physical oceanography of the southeast Asian wateres. NAGA Rep. 2, Scripps Inst. Of Oceanogr., La Jolla, CA. pp 195.

THIS PAGE INTENTIONALLY LEFT BLANK

INITIAL DISTRIBUTION LIST

1. Defense Technical Information Center
   Ft. Belvoir, Virginia

2. Dudley Knox Library
   Naval Postgraduate School
   Monterey, California

3. Dr. S. R. Ramp
   Department of Oceanography
   Monterey, California

4. Dr. L. K. Rosenfeld
   Department of Oceanography
   Monterey, California

5. Dr. Glen Gawarkiewicz
   Department of Physical Oceanography
   Woods Hole Oceanographic Institution
   Woods Hole, Massachusetts

6. D. Timothy Duda
   Department of Physical Oceanography
   Woods Hole Oceanographic Institution
   Woods Hole, Massachusetts

7. Dr. Tswen-Yung (David) Tang
   Institute of Marine Sciences
   Taipei, Taiwan

8. Dr. Joe Wang
   Institute of Marine Sciences
   Taipei, Taiwan

9. Dr. Dong-Shan Ko
   Naval Research Laboratory
   Oceanography Division
   Stennis Space Center, Mississippi

10. Dr. Mary L. Batteen, Chair
    Department of Oceanography
    Monterey, California